Garnet zoning as a window into the metamorphic evolution of a crystalline complex: the northern and central Austroalpine Ötztal-Complex as a polymorphic example

PETER TROPPER[1] & ARNO RECHEIS[1]

11 Figures and 9 Tables

Contents

Abstract

The Variscan and Eo-Alpine metamorphic events in the central and northern Austroalpine Ötztal Complex (ÖC) and the Schneeberg Complex (SC) were studied on a regional scale by means of interpretations of different zonation types in garnets in combination with P-T estimates, based on multi-equilibrium methods. The Variscan metamorphic event can best be studied in the northwestern part of the ÖC, because further to the southeast, the grade of the subsequent Eo-Alpine metamorphic overprint increases, culminating in pressure-dominated amphibolite-facies conditions (8-10 kbar) in the SC and eclogite facies conditions south of the SC. The investigations of the different types of garnet zoning yields 2 major groups of zonations: (1) continuous and (2) discontinuous zoning types. The first type appears in most samples of this investigation, displaying the typical "bell-shaped" elemental distribution with Ca- and Mn-rich cores. Based on geochronological data they can clearly be related to the dominant Variscan metamorphic overprint. The second type occurs in the samples of this investigation only in the southeastern part of the ÖC, adjacent to the north of the SC. This type is clearly related to the polymetamorphic history, thus providing informations on the Variscan and Eo-Alpine event. Furthermore almost all garnets display Mn-enrichment in the rims, related to either later retrogression by diffusive loss of Mg or reactions involving the grossular and pyrope component after the thermal peak of the metamorphic event. The Mn-enrichment is strongest in the western part of the ÖC and decreases towards the southeast, thus samples adjacent to the SC lack the Mn-enrichment in the rims due to Eo-Alpine overgrowth. The investigated metapelites contain the assemblage garnet + staurolite + biotite + muscovite + plagioclase ± kyanite ± sillimanite. They were used to reconstruct the peak pressure and temperature conditions with two methods: (1.) multi-equilibrium methods (THERMOCALC v. 2.7.) and (2.) the inverse chemical equilibrium approach (WEBINVEQ). For the Variscan metamorphic event, conditions of 621-708°C and 5.7-8.1 kbar were derived for garnet rim compositions to the west of the Eo-Alpine chloritoid-in isograd. The Eo-Alpine P-T conditions obtained from the ÖC range from 469°C and 4.2 kbar in the northern ÖC underneath the Permoscythian cover sequence (PC) of the Kalkkögel to 556°C and 8.8 kbar in the southern ÖC adjacent to the SC. The highest Eo-Alpine pressures were obtained from the samples of the SC and PC with 9.3-9.8 kbar at 551-574°C. The highest pressures of >10 kbar were obtained in samples from the SC and the adjacent Permoskythian cover sequence (PC). P-T data from the basement south of the Passeier-Jaufen Line, the Meran Mauls Basement (MMB) yield 540-640°C and 5.4-6.1 kbar, which can be attributed to the Variscan metamorphic event based on geochronological evidence from literature data. The data do not indicate any zoning of Variscan P-T conditions within the ÖC and confirm the increase in the Eo-Alpine P-T conditions towards the SC and the lack of Eo-Alpine metamorphic overprint, higher than greenschist facies, in the crystalline basement south of the Passeier-Jaufen Line.

Address of the authors
_____

[1] Peter TROPPER and Arno RECHEIS, Institute of Mineralogy and Petrography, University of Innsbruck, Innrain 52, A-6020 Innsbruck, Austria
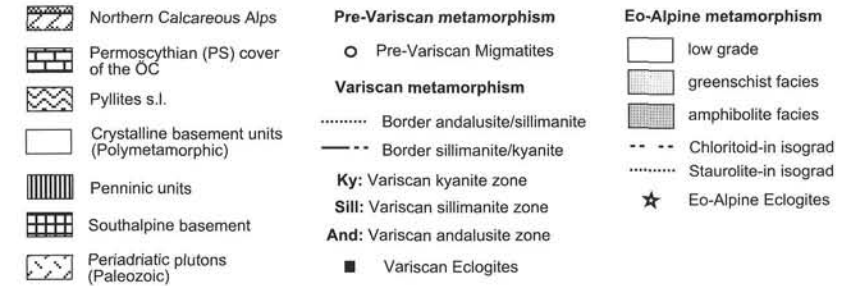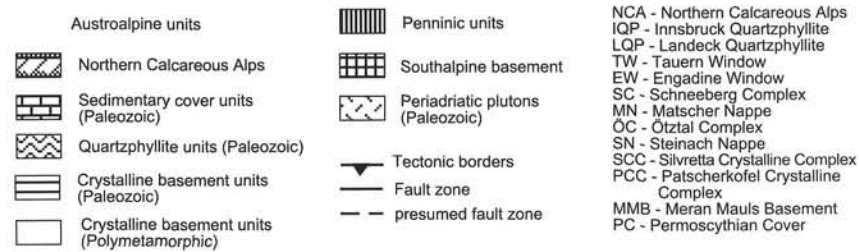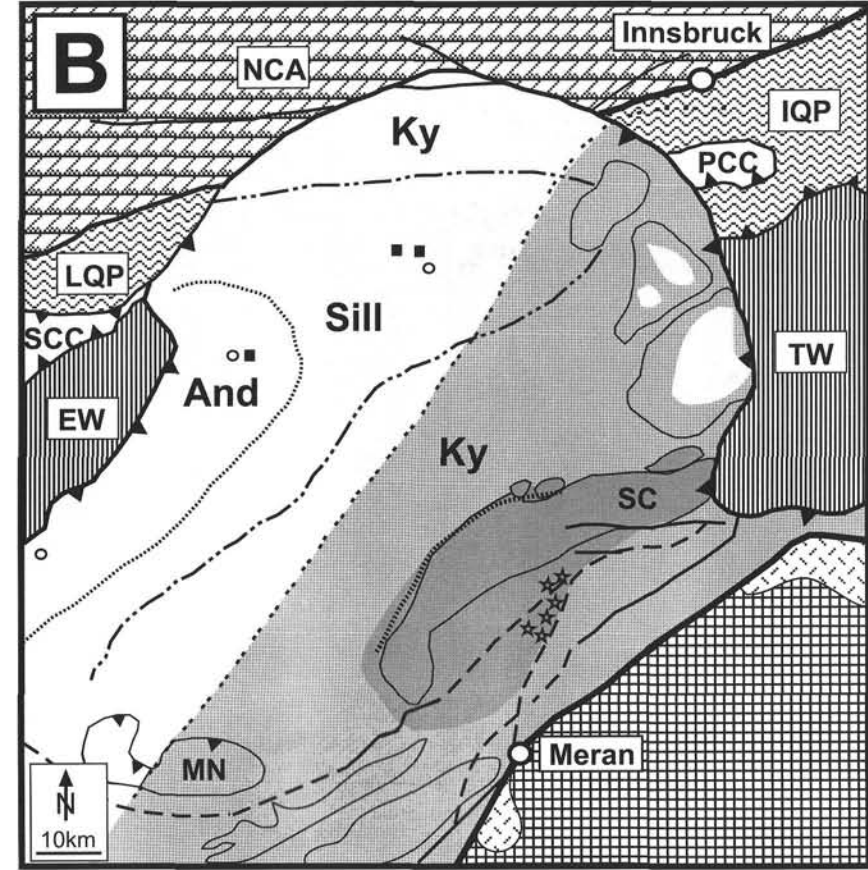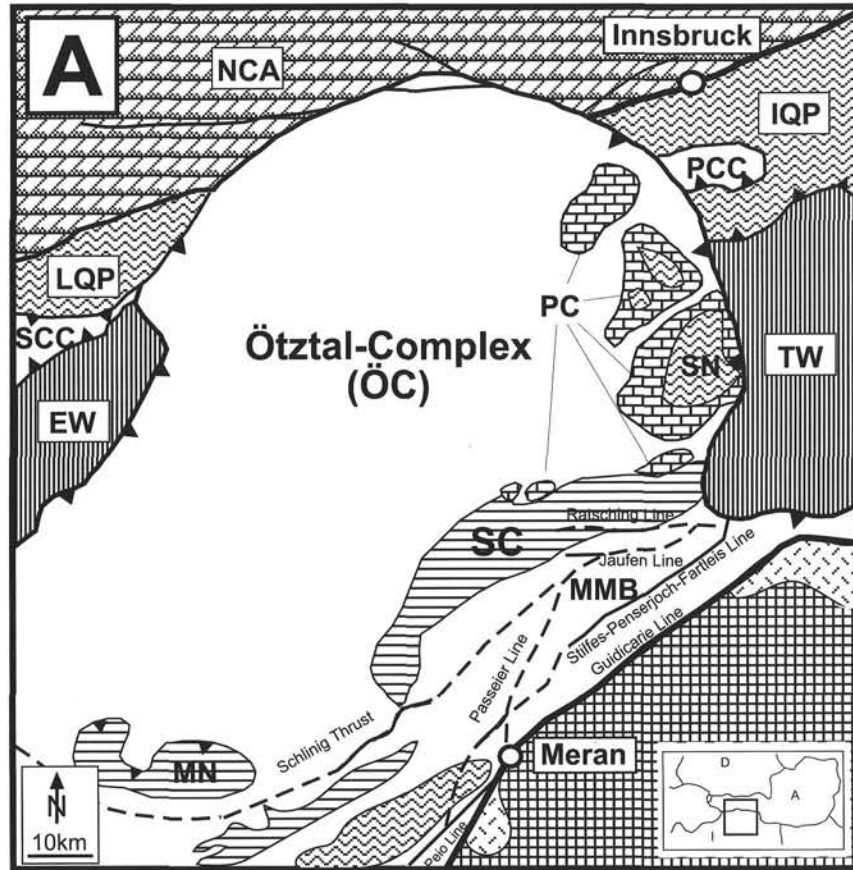
1. Introduction

Since the late 60's, garnet zoning was recognized as a useful tool in deciphering the metamorphic history of crystalline rocks (TRACY, 1982). In the Eastern Alps, the Austroalpine basement typically shows polymetamorphism due to a sequence of metamorphic overprints, affecting this part of the Alps. The most dominant metamorphic overprints are the Variscan- and the Eo-Alpine metamorphic event (HOINKES et al., 1999; NEUBAUER, 1999; THÖNI, 1999). In recent years, geochronological data also point to a widespread Permian thermal overprint mainly observed in the eastern part of the Austroalpine units (SCHUSTER et al., 2001).

The Ötztal Complex (ÖC) is a large crystalline complex in the western part of the Austroalpine units (Fig. 1A). Petrological as well as geochronological data indicate at least three

Fig. 2
Regional distribution of the sample localities of this investigation. Legend is the same as in Figure 1A.

periods of metamorphism: First, a "Caledonian" event (490-420 Ma) resulting in the local formation of migmatites (SÖLLNER and HANSEN, 1987; CHOWANETZ, 1990, CHOWANETZ, 1991, CHOWANETZ, 1994, SCHWEIGL, 1995; KLÖTZLI-CHOWANETZ et al., 1997; KLÖTZLI-CHOWANETZ, 2001), second a dominant Variscan amphibolite facies event (390-295 Ma, LICHEM, 1993; SCHWEIGL, 1995; HOINKES et al., 1997) and last, the Eo-Alpine event from 100 to 73 Ma (HOINKES and THÖNI, 1993; THÖNI, 1999; EXNER et al., 2001; HABLER et al., 2001). The degree of the Eo-Alpine metamorphic overprint in the ÖC increases from greenschist facies conditions in the northwest to pressure-dominated amphibolite-facies conditions north of the SC to eclogite facies conditions in the southeast of the SC as shown in Figure 1B (HOINKES, 1986a; HOINKES et al., 1991; KONZETT and HOINKES, 1996). Especially in the northwest, some areas almost completely escaped the Eo-Alpine overprint allowing to study the P-T conditions of the Variscan metamorphic event (TROPPER and HOINKES, 1996; HOINKES et al., 1997).

In the ÖC, the Eo-Alpine metamorphic event is better understood than the pre-Alpine metamorphic evolution in terms of geochronology and metamorphic conditions, due to large amount of petrological and geochronological data (PURTSCHELLER et al., 1981; HOINKES, 1981; HOINKES and THÖNI, 1983; FRANK et al., 1987; NEUBAUER et al., 1999; THÖNI, 1999). The pre-Alpine metamorphic event has been studied in metapelites only on samples from scattered localities mostly from the western ÖC (VELTMAN, 1986; BERNHARD et al., 1993; BERNHARD, 1994; KAINDL, 1995; LICHEM, 1993; TROPPER and HOINKES, 1996). Since the thermobarometric constraints of the Variscan metamorphism were obtained so far mostly from the western and northern part of the ÖC, it was therefore the aim of this contribution to focus on the pre-Alpine metamorphic evolution on a larger scale, by investigating samples from a large area of the ÖC which covers the Austrian part of the ÖC and reaches into the Italian part in the southeast, ranging from areas in the north-
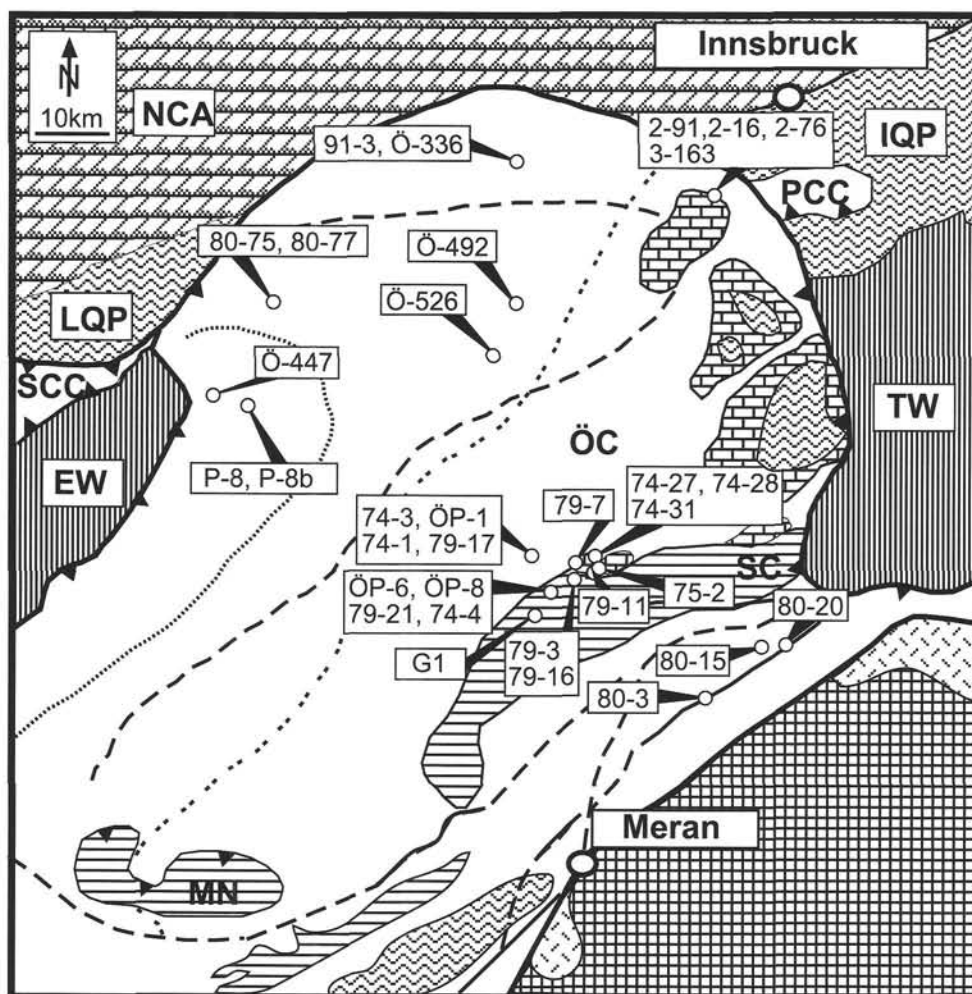
← Fig. 1
Geological (A) and petrological (B) overview over the Ötztal Complex (ÖC). (A) The samples are from the ÖC, SC, MMB and the sedimentary cover units of the ÖC, the Permoscythian Cover (PC). (B) The petrological overview is only shown for the ÖC and not its neighboring units. The distribution of the Variscan aluminiumsilicates is according to PURTSCHELLER (1969). The chloritoid-in isograd is from HOINKES et al. (1982). The staurolite-in isograd is from HOINKES (1981). The distribution of the pre-Variscan migmatites is from KLÖTZLI-CHOWANETZ (2001). The extent of the Eo-Alpine metamorphic overprint was taken from the metamorphic map of the Alps by FREY et al. (1999).

west where Eo-Alpine metamorphism is almost lacking, to the south where the dominant Eo-Alpine metamorphic overprint occurs (Fig. 2). VELTMAN (1986) and RECHEIS (1998) started to investigate garnet zonations from different parts of the ÖC. These studies provide the basis for our investigation. Thus, our aim is not only to provide additional information on the pre-Alpine P-T evolution by combining garnet zoning data and thermobarometric estimates to provide a large scale reconstruction of the Variscan metamorphic history but also to investigate the Eo-Alpine metamorphic overprint.

2. Geological Setting and metamorphic evolution of the ÖC

The ÖC is part of the Austroalpine basement nappes in the Eastern Alps (FRANK et al., 1987) and is tectonically emplaced over Penninic units during the Alpine event. The Penninic units are exposed in the Tauern Window and the Engadin Window and border the ÖC to the east and west and the borders of the ÖC are the Brenner Line in the east and the Engadine Line in the west. The Northern Calcareous Alps (NCA) are the border to the north and the Schlinig Line from the upper Vintschgau to the Schnalstal is the southern border (Fig. 1A). Near the Schnalstal, west of Meran, it is impossible to define unambiguously the eastward continuation of the Schlinig Thrust. Photo lineaments analyses based on satellite images indicate a possible continuation to the junction of the Passeier Line with the Jaufen Line (KÖHLER, 1978). Based on petrological investigations, the eastward continuation of the southern border of the ÖC runs along the Etsch Valley and then follows the Passeier and Jaufen Lines near Meran up to the Brenner Line (HOINKES and THÖNI, 1993). The ÖC represents the basement unit for the following units: the Schneeberg Complex (SC) represents remnants of a Paleozoic metasedimentary cover on top of the basement of the ÖC, the Matsch nappe in the southern part of the ÖC represents an allochthonous Paleozoic metasedimentary sheet unit and the Steinacher nappe in the eastern part of the ÖC also represents a Paleozoic metasedimentary unit. The Steinacher nappe shows a normal fault contact to the remnants of the underlying Permoscythian cover sequences (PC) of the ÖC. Latter occur along the western side of the Brenner Line, at the northern margin of the SC and immediately to the south of the Stilfes-Penser Joch-Fartleis Line. Lithological similarities of the crystalline basement between the Passeier-Jaufen line and the Periadriatic line with the ÖC led to the inclusion of this area to the ÖC and hence definition of the Guidicarien line as the southeastern border of the ÖC. On the other hand, due to the differences in the Eo-Alpine metamorphic evolution between the crystalline basement north and south of the Passeier-Jaufen line, the area south of this fault zone is considered to be a different crystalline basement, called the Meran-Mauls Basement (SPIESS, 1995) or Mauls-Penserjoch-Complex (SÖLVA et al. 2001). In this paper we also consider this crystalline basement as a separate basement unit, called the Meran-Mauls Basement (MMB).

The ÖC consists of quartzofelspatic and metapelitic metasediments with various intercalations of orthogneisses, amphibolites and rare metacarbonates. The oldest

metamorphic event is "Caledonian" in age (460-490 Ma), leading to the formation of orthogneisses (THÖNI, 1986) and scattered occurrences of migmatites as shown in Figure 1B (SÖLLNER et al., 1982; SÖLLNER and SCHMIDT, 1993; CHOWANETZ et al., 1997). HOINKES (1973) estimated the P-T conditions of migmatite formation with 680°C and ≥4 kbar. The Variscan metamorphic overprint ranges from 390-295 Ma (THÖNI, 1999). The first stage of the Variscan event was a high pressure metamorphism around 373-359 Ma, leading to the formation of eclogites in the central part of the ÖC (MILLER and THÖNI, 1995). The conditions of the eclogite facies were estimated to be 710-748°C and 26.7-27.9 kbar (MILLER and THÖNI, 1995). The dominant amphibolite facies metamorphism occurred around 330-350 Ma, as evident from Sm-Nd garnet-whole rock ages from mica schists (SCHWEIGL, 1993; HOINKES et al., 1997; THÖNI, 1999; THÖNI, 2002). PURTSCHELLER (1969) observed on the basis of the regional distribution of Al_2SiO_5 polymorphs in metapelites a systematic regional zonation and distinguished within the ÖC two zones: (1.) the southern and northern kyanite zone and (2.) the central sillimanite zone including the andalusite zone in the west (Fig. 1B). HOINKES and THÖNI (1993) pointed out that the occurring mineral zonation does not have to be the consequence of a single Variscan metamorphic event. VELTMAN (1986) estimated metamorphic P-T conditions in metapelites for the sillimanite zone of 610-670°C and 4-8 kbar and for the northern kyanite zone 570-610°C and 4-8 kbar. TROPPER and HOINKES (1996) estimated P-T conditions of 570-640°C and 5.8-7.5 kbar for the northwestern part of the ÖC.

The youngest metamorphic event in this Austroalpine basement occurred during the Cretaceous Eo-Alpine orogeny (100-73 Ma, THÖNI, 1981; THÖNI, 1999; EXNER et al., 2001; HABLER et al., 2001). The intensity of the Eo-Alpine overprint varies within the ÖC and increases from NW (lower greenschist facies) to SE (epidote-amphibolite facies) and reaches 550-600°C and ≥11 kbar in the Schneeberg Complex as shown in Figure 1B (HOINKES et al., 1991; KONZETT and HOINKES, 1996). This zonation ends abruptly at the Passeier-Jaufen Line. This leads also to resetting of Variscan cooling ages from the NW to the SE (THÖNI 1981; THÖNI, 1999). To the south of the Passeier-Jaufen Line, in the Meran-Mauls basement (MMB) only a weak Eo-Alpine metamorphic overprint can be detected (SPIESS, 1995).

This investigation represents the continuation of the work of VELTMAN (1986), who started to investigate variations of garnet zoning types within the ÖC and therefore we chose samples of garnet-bearing metapelites from 15 localities within the northern and central ÖC, the SC, the PC and the area to the south of the Passeier-Jaufen Line the Meran-Mauls Basement, MMB, (Fig. 2) to correlate garnet zoning types and thermobarometric estimates from a large area of the western Austroalpine nappes.

3. Textural relations and Petrography

Textural relationships: The samples of this investigation are from the Austrian as well as the southeastern Italian part of the ÖC as shown in Figure 2 and Table 1. The samples are all metapelites, containing garnet porphyroblasts and rich in amphibolite facies index minerals such as staurolite and kyanite. Due to intense ductile deformation, the sam-

Table 1
Mineral assemblages from the Ötztal Basement (ÖB), the Permoscyth cover sequence (PS) and the Schneeberg Complex (SC).

Sample	Locality	Mineral assemblage	Grt inclusions	Alteration minerals	Accessory minerals	Unit	TB
91-3	Kreuzjoch	Grt + St + Bt + Pl + Ms + Qtz	Qtz, Rt	Chl, Ser	Rt + Ilm + C + Zirc	ÖC	x
Ö-336	Kreuzjoch	Grt + St + Bt + Pl + Ms + Qtz	Qtz, Rt, C	Zo + Ab	Rt + Ilm + C	ÖC	
2-16	Kalkkögelbasis	Grt + St + Bt + Pl + Ms + Qtz	Pl, Qtz, Ilm	Chl, Ser	Ilm + Ap	ÖC	
2-76	Kalkkögelbasis	Grt + Bt + Pl + Ms + Qtz	-	Chl + Ser + Zo + Ab	Ilm + Zirc	ÖC	
2-91	Kalkkögelbasis	Grt + Bt + Pl + Ms + Qtz	Qtz, C(?), FI	Chl + Zo + Ab + Ser	Rt + Ilm + Tur	ÖC	x
3-163	Kalkkögelbasis	Grt + Bt + Pl + Ms + Qtz	-	Chl + Ser + Ttn	Rt + Ilm + Ap	ÖC	
80-75	Tumpen Alm	Grt + St + Ky + Sill + Bt + Pl + M + Qtz	Bt, Pl, Ms, Qtz, C, FI	Chl + Ser	Ilm + Ttn + C	ÖC	
80-77	Tumpen Alm	Grt + St + Ky + Sill + Bt + Pl + Ms + Qtz	Ms, Qtz, C	Chl + Ser	Rt + Ilm + C + Zirc + Aln	ÖC	x
Ö-492	Zischkeles	Grt + St + Sill + Bt + Pl + Ms + Qtz	Ky, Ilm, Qtz	Chl	Rt + Ilm + Tur + Zirc + Ttn	ÖC	x
Ö-526	Hinteres Langental	Grt + St + Bt + Pl + Ms + Qtz	Qtz, Ilm, Rt	Chl + Zo + Ab + Ser	Rt + Ilm + C + Aln	ÖC	x
P-8	Aifner Spitze	Grt + Bt + Pl + Qtz	Bt, Ms, Rt, Ilm, Qtz, C	Chl + Ser	Rt + Ilm + Ap + Aln	ÖC	
P-8b	Aifner Spitze	Grt + Bt + Pl + Ms + Qtz	Bt, Ms, Rt, Ilm, Qtz, C	Chl + Ser	Rt + Ilm + Ap + Aln	ÖC	x
Ö-447	Aifner Spitze/Ölgrubenjoch	Grt + St + Ky + Bt + Pl + Ms + Qtz	St, Rt, Ilm, Ms, C, Tur	Chl + Ser	Rt + Ilm + Tur + Aln	ÖC	
ÖP-1	Timmelsjoch	Grt + Bt + Pl + Ms + Qtz	Bt, Qtz, Ilm, Zirc	Chl + Ser + Zo + Ab	Rt + Ttn + Ap + Tur + Aln	ÖC	
74-3	Timmelsjoch	Grt + Bt + Ky + Mus + Pl + Qtz	Bt, Qtz, C, FI(?)	Chl	Rt + Ilm + Ap + Aln	ÖC	x
74-1	Timmelsjoch	Grt + Bt + Pl + Ms + Qtz	Qtz, Rt, C	Chl + Ser	Rt + Ilm + Aln	ÖC	
79-17	Timmelsjoch	Grt + Bt + Pl + Ms + Qtz	Qtz, Ilm	Chl + Ser	Rt + Ilm + Ttn	ÖC	
75-2	Egentenjoch	Grt + Bt + Pl + Ms + Qtz	Ky(?), Qtz, Ilm, FI, C	Chl + Ser + Ttn	Ilm + C + Zirc + Aln	ÖC	x
79-11	Schwarzseescharte	Grt + Bt + Pl + Ms + Qtz	Pl, Ms, Qtz, Rt, Ilm, C	Chl	Rt + Ilm	ÖC	x
79-16	Schwarzseescharte	Grt + Ky + Bt + Pl + Ms + Qtz	Ky, Rt, Ilm, C	Chl	Rt + Ilm + Tur + C	ÖC	
80-3	Unterbergtal/Alpler Alm	Grt + St + Ky + Pl + Ms + Qtz	FI, C	Chl + Ser + Zo + Ab	Ilm + Tur + Ap	MMB	x
80-15	Traminalm	Grt + St + Ky + Bt + Pl + Ms + Qtz	FI, C	Chl + Ser	Rt + Ilm + Tur + C	MMB	x
80-20	Penserjoch	Grt + St + Ky + Bt + Mu + Qtz	Bt + Qtz	Chl	Ilm + Tur	MMB	
74-28	Egetenjoch	Grt + Bt + Pl + Ms + Qtz	C + Ilm + Bt + Qtz	Chl	Ilm + Tur	PC	x
74-31	Egetenjoch	Grt + Bt + Pl + Ms + Qtz	Qtz + Tur + Ilm	Chl	Ilm + Rt + Fe-oxide	PC	
79-7	Schwarzseescharte	Grt + Bt + Ms + Qtz	Qtz + Ilm	Chl	Ilm + Zirc	PC	
74-27	Egetenjoch	Grt + Bt + Pl + Ms + Qtz	-	Chl	Ilm + Tur	PC	
79-21	Timmelsjoch	Grt + Bt + Pl + Ms + Qtz	Ky(?) + Qtz + Ilm	Chl	Rt + Ilm	SC	
ÖP-6	Timmelsjoch	Grt + Bt + Pl + Ms + Qtz	Rt + Bt + Ilm	-	Rt + Ilm + Tur	SC	
74-4	Timmelsjoch	Grt + Bt + Ms + Qtz	Qtz + Ilm + Rt	-	Rt + Ilm + Zirc + Aln	SC	
ÖP-8	Timmelsjoch	Grt + Bt + Pl + Ms + Qtz	Qtz + Ilm	Chl	Ilm + Tur	SC	
79-3	Schwarzseescharte	Grt + Bt + Pl + Ms + Qtz	C + Qtz + Ilm	Chl + Ser	Rt + Ilm + Zirc	SC	x

Abbreviations after Kretz (1983), except for FI: fluid inclusion; Ser: sericite; TB: thermobarometry and x indicates if the sample was used for *P-T* estimations. ÖC: Ötztal Complex; MMB: Meran-Mauls Basement; SC: Schneeberg Complex; PC: Permoscythian Cover sequence.

ples are strongly foliated and also show internal folding. Usually muscovite and biotite form the foliation. Some garnets appear to be rotated, thus containing an internal schistosity, mostly made of ilmenite, quartz or graphite. Some staurolite crystals, also show a similar feature. Large crystals of kyanite, staurolite and plagioclase overgrow sometimes the matrix. The texture is lepidoblastic, but with increasing garnet content it becomes more porphyroblastic. The Ti-bearing accessory minerals like rutile and ilmenite usually occur together as inclusions in staurolite and garnet. In the matrix, ilmenite is the dominant Ti-bearing mineral. The following mineral assemblages are observed (Table 1):

1. Garnet + Staurolite + Kyanite + Biotite + Muscovite + Plagioclase + Quartz
2. Garnet + Staurolite + Kyanite + Sillimanite + Biotite + Muscovite + Plagioclase + Quartz
3. Garnet + Staurolite + Biotite + Muscovite + Plagioclase + Quartz
4. Garnet + Kyanite + Biotite + Muscovite + Plagioclase + Quartz
5. Garnet + Biotite + Muscovite + Plagioclase + Quartz
6. Garnet + Biotite + Plagioclase + Quartz

Almost all samples contain additionally apatite, zircon, allanite and tourmaline as accessory phases.

3.1 Petrography of the major constituents

Garnet occurs as porphyroblasts in a mica-rich matrix and contains mostly muscovite, quartz, rutile, ilmenite and plagioclase inclusions (Table 1). Only garnets from three samples contain petrologically important minerals: one sample (Ö-447) contains staurolite inclusions and two samples (Ö-492; 79-16) contain kyanite inclusions. Many samples also show garnets with cloudy cores, probably stemming from graphite inclusions. *Staurolite* occurs mostly as idiomorphic porphyroblasts, which often contain garnet, biotite, rutile, quartz and graphite inclusions. Staurolite is also frequently intergrown with kyanite. *Kyanite* appears as elongated idioblastic crystals and is considered to be the equilibrium Al_2SiO_5 modification because it shows equilibrium textures with the coexisting KFMASH-phases staurolite, garnet, biotite and muscovite. Garnet also occurs as inclusion in kyanite together with biotite, quartz and rutile (sample 80-15). Two samples (Ö-492, 80-77) show a transformation of biotite to sillimanite, which is a common feature from the northwestern part of the ÖC during later stages of the *P-T* path (TROPPER and HOINKES, 1996). *Plagioclase* forms usually large porphyroblasts, overgrowing the matrix. These porphyroblasts are optically and chemically unzoned. In some samples, small crystals of optically and chemically zoned plagioclase appear. *Biotite* and *muscovite* occur along the schistosity of the samples. Retrograde features, such as replacement of biotite by chlorite and plagioclase by albite and zoisite and sericite are also common.

4. Mineral Chemistry

Electron microprobe analyses of minerals were performed on an ARL-SEMQ microprobe at the Institute of Mineralogy and Petrography at the University of Innsbruck. Analytical conditions were 15 kV and a sample current of 20 nA on brass. Most data were obtained with point mode. Mica and feldspar were analyzed using 10×10 μm raster. The data were reduced with the program MacQuant (MERSDORF, 1992 unpubl.) with the empirical correction method by BENCE and ALBEE (1968) and improved alpha factors of EVANS (1978 unpubl.) and MERSDORF (unpubl.). Natural and synthetic standards were used to calibrate the microprobe prior to analysis. Additional to wavelength dispersive analysis (WDS), energy dispersive analysis (EDS) were also performed. The analyses were obtained on a NORAN-Voyager EDS system, which was calibrated with synthetic elemental standards. The formulae of garnet, biotite, muscovite, plagioclase and ilmenite were calculated with the program MacAX (HOLLAND, 1999, written comm.). Staurolite formulae were calculated with the program HYPERFORM96 (BJERG et al., 1996).

Garnet: All garnets are almandine rich (Alm_{60-80}) with small amounts of pyrope- (Pyr_{3-12}), grossular- (Gro_{2-25}) and spessartine- ($Spe_{0.5-15}$) components (Table 2). Based on the chemical data, several types of zoning were observed (Fig. 3). The regional distribution of garnets from representative samples is shown in Figure 4. The chemical zoning profiles of all garnets are shown in Figure 4 and in the Appendix.

Type 1, normal continuous zoning: Within this group, three types can be distinguished which are schematically shown in Figure 3A: (1) Mn and Ca enrichment in the core (Type 1 MnCa). This type is the most common zoning type in the ÖC (Table 3). This type is comparable to type 1 of VELTMAN (1986) as shown in Figure 3B. Sample ÖP-8 shows a typical continuous zoning with increasing Mg/(Mg+Fe^{2+}) and X_{Alm} and decreasing X_{Gro} and X_{Spe} from the core to the rim from Gro_7 to Gro_1 and Spe_8 to Spe_0 (Fig. 5A). (2) Mn enrichment in the core (Type 1 Mn). Some garnets show a plateau-like distribution of MgO and CaO in the core, whereas MnO and FeO behave conversly (Fig. 5B, sample 79-21). (3) Ca enrichment in the core (Type 1 Ca). Garnets from the sample ÖP-6 show a plateau-like distribution of MnO and MgO in the cores whereas CaO shows a decrease from the core to the rim and FeO behaves conversely (Fig. 5C).

Type 2, invers continuous zoning: This type is comparable to type 2 of VELTMAN (1986) as shown in Figure 3B. These garnets have been found only in two sample from the base of the Permoscythian cover sequence in the northern part of the ÖC. They show constant core compositions and a significant decrease of the almandine component and an increase of the spessartine component within the outermost 50 μm (Fig. 4, samples 2-91, 2-16). The grossular content is low (Gro_{6-7}) and constant throughout the garnet.

Type 3, discontinuous zoning: This type is comparable to type 3 in Figure 3B of VELTMAN (1986). In most cases there is a correlation between optical (inclusion-rich core) and chemical zoning. Sample 74-1 shows a typical example of this zoning type (Fig. 5D). These garnets show a homogenous composition in the core and a sudden change in composition towards the rims. The grossular content increases strongly from Gro_8 to Gro_{25}, whereas the almandine and pyrope content decrease from Alm_{76} to Alm_{65} and Pyr_{11} to Pyr_9. In contrast to the discontinuous zoning of the other components, spessartine shows a continuous zoning and decreases slightly towards the rim of the garnet from Spe_5 to Spe_2. The abrupt change in chemical composition takes place over a distance of 5 μm. Other samples in the Appen-
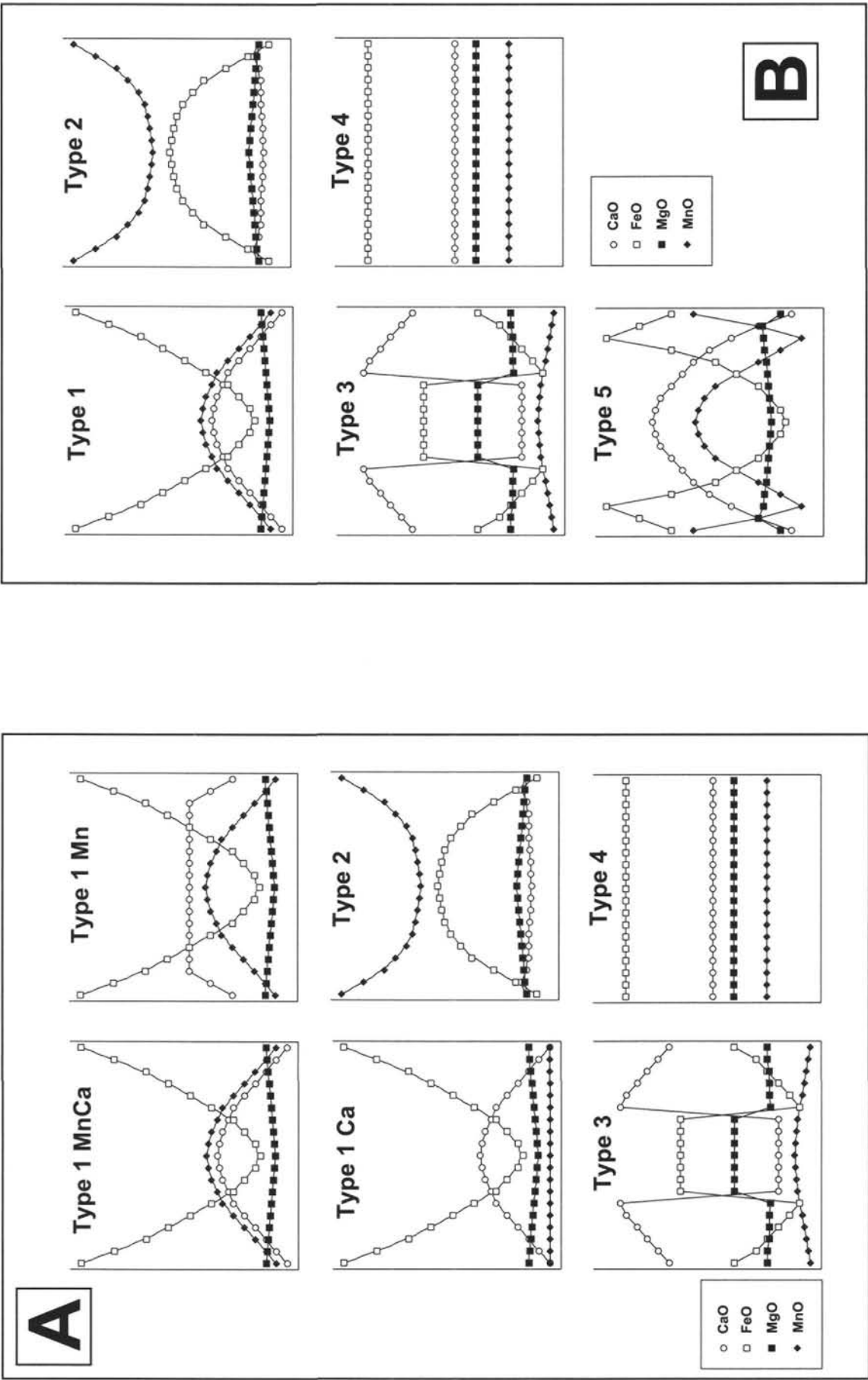
Fig. 3
Idealized overview over the garnet zoning types according to (A) RECHEIS (1998) and (B) VELTMAN (1986).

Table 2
Representative microprobe analyses of garnet.

Sample	Ö-492 core	Ö-492 rim	Ö-492 outer rim	P-8b core	P-8b rim	P-8b outer rim	ÖP-1 core	ÖP-1 rim	2-91 core	2-91 rim	74-1 core	74-1 rim
SiO_2	36.65	36.44	36.10	36.50	36.82	36.46	36.30	36.88	36.49	36.30	36.76	37.07
TiO_2	0.04	n.d.	n.d.	0.15	0.07	0.02	n.d.	0.05	n.d.	n.d.	n.d.	0.09
Cr_2O_3	n.d.	0.34	0.02	0.01	0.01	n.d.	n.d.	0.02	n.d.	0.28	0.04	0.05
Al_2O_3	20.57	20.98	20.40	20.38	20.89	21.30	21.08	21.24	20.65	20.33	20.68	20.95
$^aFe_2O_3$	1.40	1.94	1.75	2.80	2.46	2.54	1.91	2.00	1.59	1.18	0.91	1.51
FeO	35.82	37.06	35.09	24.93	29.19	28.38	30.96	33.19	32.10	32.17	32.69	29.58
MnO	2.09	0.28	3.80	6.82	0.82	7.66	1.68	0.75	3.98	4.53	2.05	0.97
MgO	2.03	3.31	2.07	0.71	2.56	2.08	1.60	2.67	2.45	1.91	2.71	2.09
CaO	1.80	0.26	0.42	8.33	7.42	2.94	6.16	4.24	2.45	2.53	3.40	7.90
Total	100.40	100.60	99.65	100.64	100.24	101.39	99.70	101.04	99.71	99.23	99.24	100.22
Si	2.972	2.935	2.960	2.938	2.939	2.917	2.936	2.939	2.963	2.973	2.982	2.961
Al	1.966	1.992	1.972	1.934	1.966	2.009	2.010	1.995	1.977	1.963	1.978	1.973
Ti	0.002	n.d.	n.d.	0.009	0.004	0.001	n.d.	0.003	n.d.	n.d.	n.d.	0.005
Cr	n.d.	0.022	0.001	0.001	0.001	n.d.	n.d.	0.001	n.d.	0.018	0.003	0.003
Fe^{3+}	0.086	0.117	0.108	0.169	0.148	0.153	0.116	0.120	0.097	0.073	0.055	0.091
$^aFe^{2+}$	2.429	2.496	2.406	1.679	1.948	1.899	2.094	2.212	2.179	2.204	2.218	1.976
Mn	0.144	0.019	0.264	0.465	0.055	0.519	0.115	0.051	0.274	0.314	0.141	0.066
Mg	0.245	0.397	0.253	0.085	0.305	0.248	0.193	0.317	0.296	0.233	0.328	0.249
Ca	0.157	0.022	0.037	0.719	0.635	0.252	0.534	0.362	0.213	0.222	0.296	0.677
Σ Cations	8.000	8.000	8.000	8.000	8.000	8.000	8.000	8.000	8.000	8.000	8.000	8.000
Almandine	0.79	0.83	0.81	0.57	0.66	0.65	0.71	0.75	0.75	0.71	0.75	0.62
Pyrope	0.06	0.15	0.09	0.03	0.10	0.08	0.06	0.11	0.09	0.09	0.12	0.09
Grossular	0.08	0.01	0.01	0.24	0.22	0.09	0.20	0.12	0.07	0.07	0.09	0.27
Spessartine	0.07	0.01	0.09	0.16	0.02	0.18	0.02	0.02	0.09	0.13	0.04	0.02

^{a}calculated; Basis of formula calculation: 12 oxygens; n.d. not detected; Type 1 garnets (continuous zoning): Ö-492; P-8b; ÖP-1; Type 2 garnet (inverse zoning): 2-91; Type 3 garnet (discontinuous zoning): 74-1
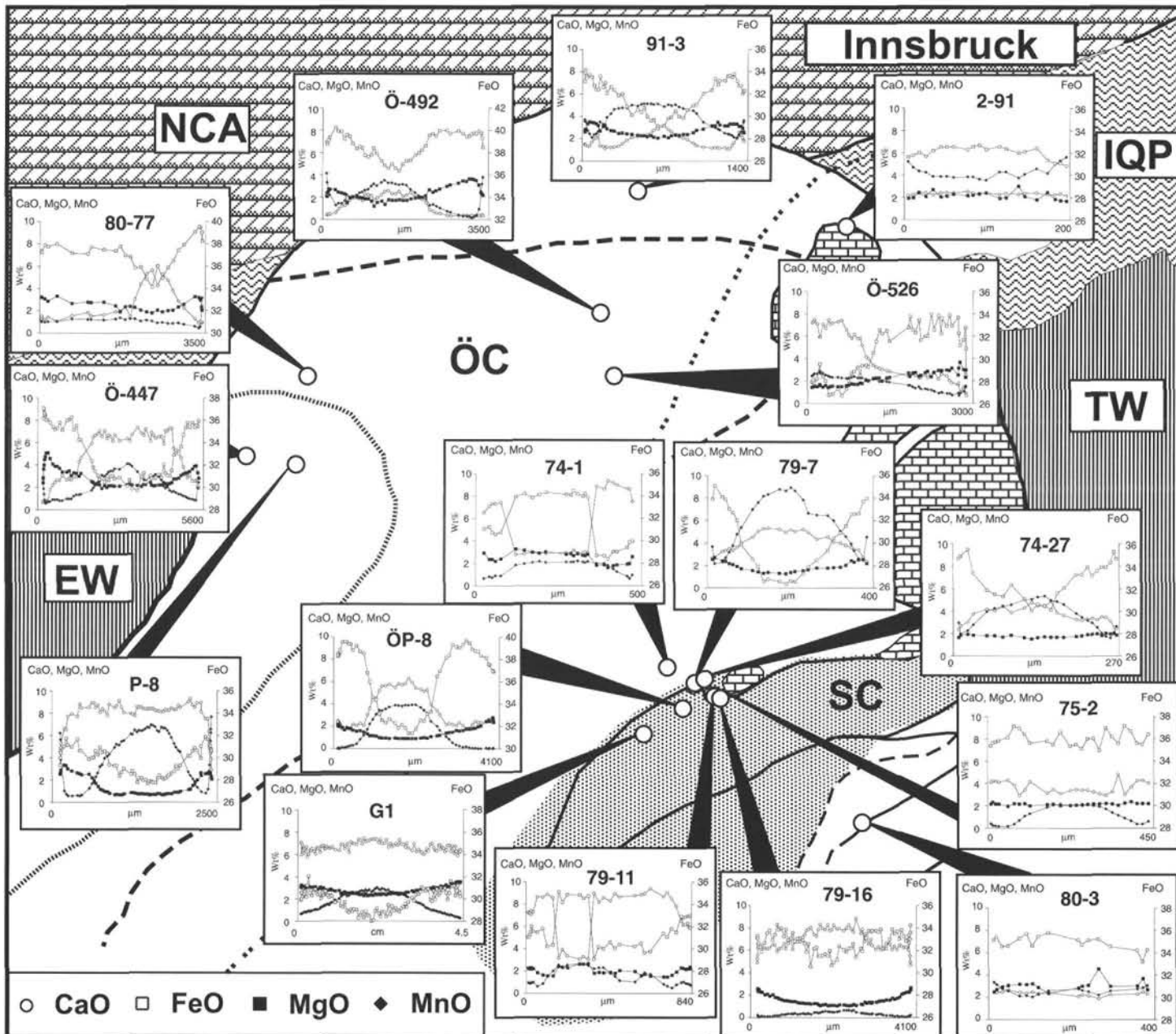
Fig. 4
Regional distribution of samples of the most prominent garnet zoning types from this investigation. Legend is the same as in Figure 1A. Sample G1 represents a zoning profile from a single garnet from the SC (Timmelsjoch) with a diameter of 8 cm (!).

ÖP-8

79-21

ÖP-6

74-1
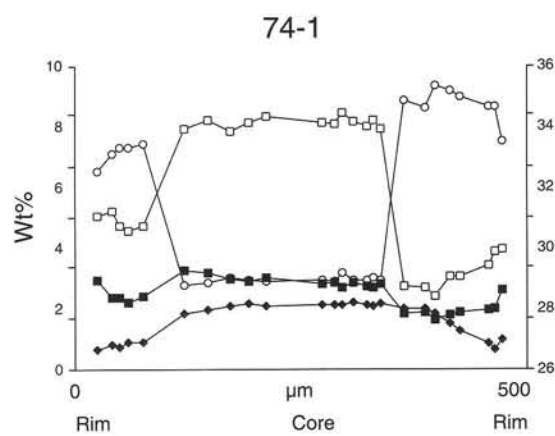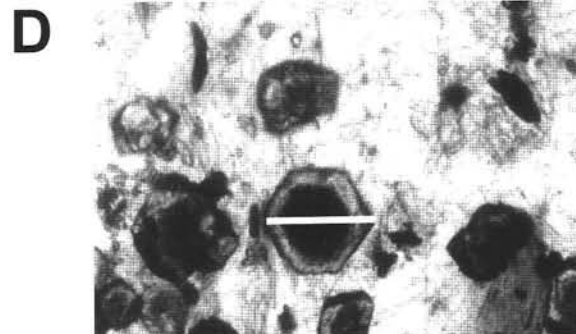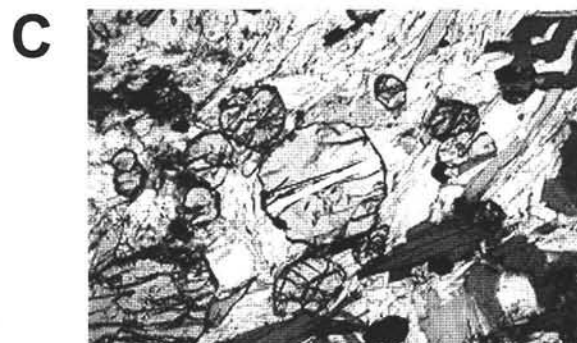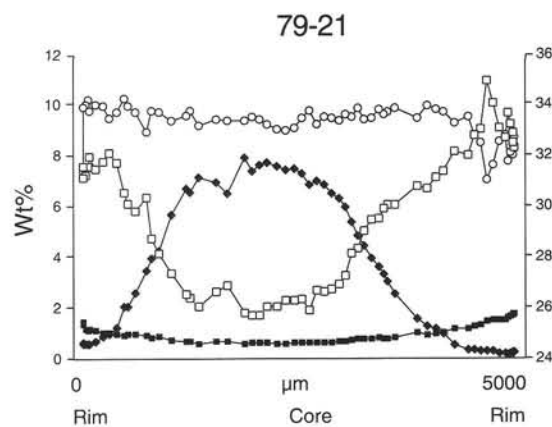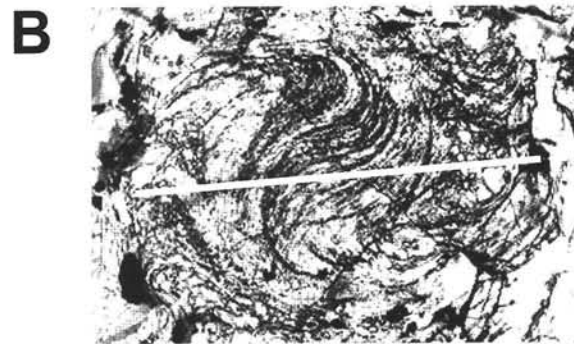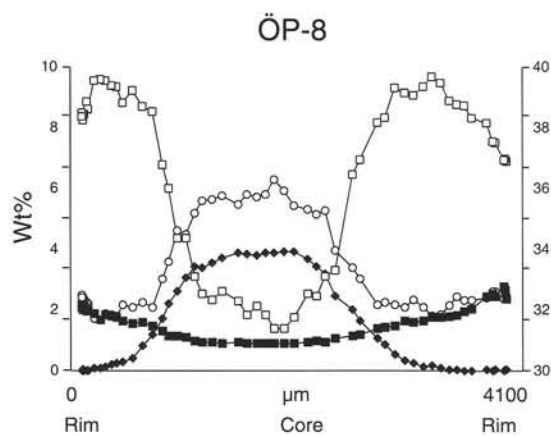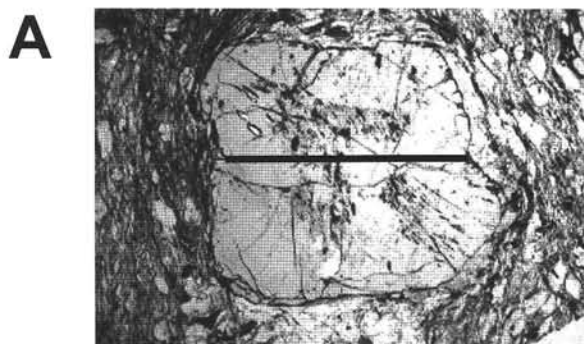
o CaO   □ FeO   ■ MgO   ◆ MnO

dix showing discontinuous zoning are samples 74-3, 74-1, 79-11 and 79-3.

Type 4, homogenous zoning: We find some samples (samples 80-3, 80-15, 80-20, P-8b, 2-76) with garnets that show zoning, comparable to zoning type 4 (homogenous zoning, Figure 3B) of VELTMAN (1986), but in contrast to his data most garnets display an increase in Mn in the outer 50 μm.

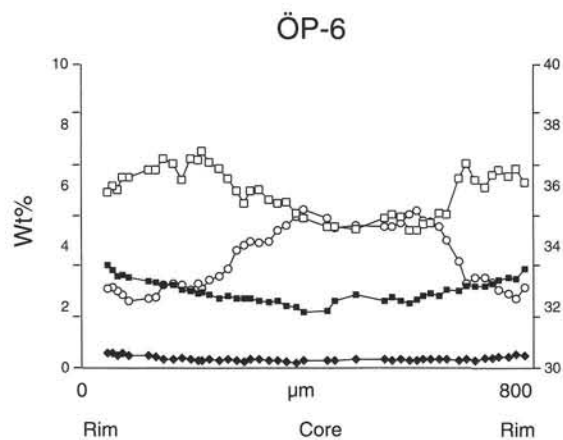Table 3 gives an overview over the garnet zoning types from this investigation and Figure 6 shows the regional distribution of examples of garnet zoning types from the investigations of VELTMAN (1986) in Figure 6A and RECHEIS (1998) in Figure 6B. Type 5 of VELTMAN (1986), displaying extreme Mn-enrichment in the rims of the garnets, was not considered as a separate garnet zoning type, since Mn-

Table 3
Overview over the garnet zoning types in this study.

Sample	Locality	Type 1	Type 2	Type 3	Type 4	Unit
91-3	Kreuzjoch	MnCa				ÖC
Ö-336	Kreuzjoch	Ca				ÖC
2-16	Kalkkögelbasis		x			ÖC
2-76	Kalkkögelbasis				x	ÖC
2-91	Kalkkögelbasis		x			ÖC
3-163	Kalkkögelbasis	MnCa				ÖC
80-75	Tumpen Alm	Ca				ÖC
80-77	Tumpen Alm	Ca				ÖC
Ö-492	Zischkeles	MnCa				ÖC
Ö-526	Hinteres Langental	Ca				ÖC
P-8	Aifner Spitze	Mn				ÖC
P-8b	Aifner Spitze				x	ÖC
Ö-447	Aifner Spitze/Ölgrubenjoch	MnCa				ÖC
ÖP-1	Timmelsjoch	Ca				ÖC
74-3	Timmelsjoch			x		ÖC
74-1	Timmelsjoch			x		ÖC
79-17	Timmelsjoch	MnCa				ÖC
75-2	Egentenjoch	Mn				ÖC
79-11	Schwarzseescharte			x		ÖC
79-16	Schwarzseescharte	MnCa				ÖC
80-3	Unterbergtal/Alpler Alm				x	MMB
80-15	Traminalm				x	MMB
80-20	Penserjoch				x	MMB
74-28	Egetenjoch	Ca				PC
74-31	Egetenjoch	Mn				PC
79-7	Schwarzseescharte	MnCa				PC
74-27	Egetenjoch	MnCa				PC
79-21	Timmelsjoch	Mn				SC
ÖP-6	Timmelsjoch	Ca				SC
74-4	Timmelsjoch	MnCa				SC
ÖP-8	Timmelsjoch	MnCa				SC
G1	Timmelsjoche	Mn				SC
79-3	Schwarzseescharte			x		SC

The garnet zoning types are according to Recheis (1998) and are explained in the text. ÖC: Ötztal Complex; MMB: Meran-Mauls Basement; SC: Schneeberg Complex; PC: Permoscythian Cover sequence.

← Fig. 5
Photomicrographs of typical garnets in metapelites and their zoning profiles: (A) continuous chemical zonation of garnet type 1 Mn, sample ÖP-8; (B) continuous chemical zonation of garnet type 1 Ca, sample 79-21; (C) continuous chemical zonation of garnet type 1 MnCa, sample ÖP-6; (D) disontinuous chemical zonation of garnet type 3, sample 74-1.
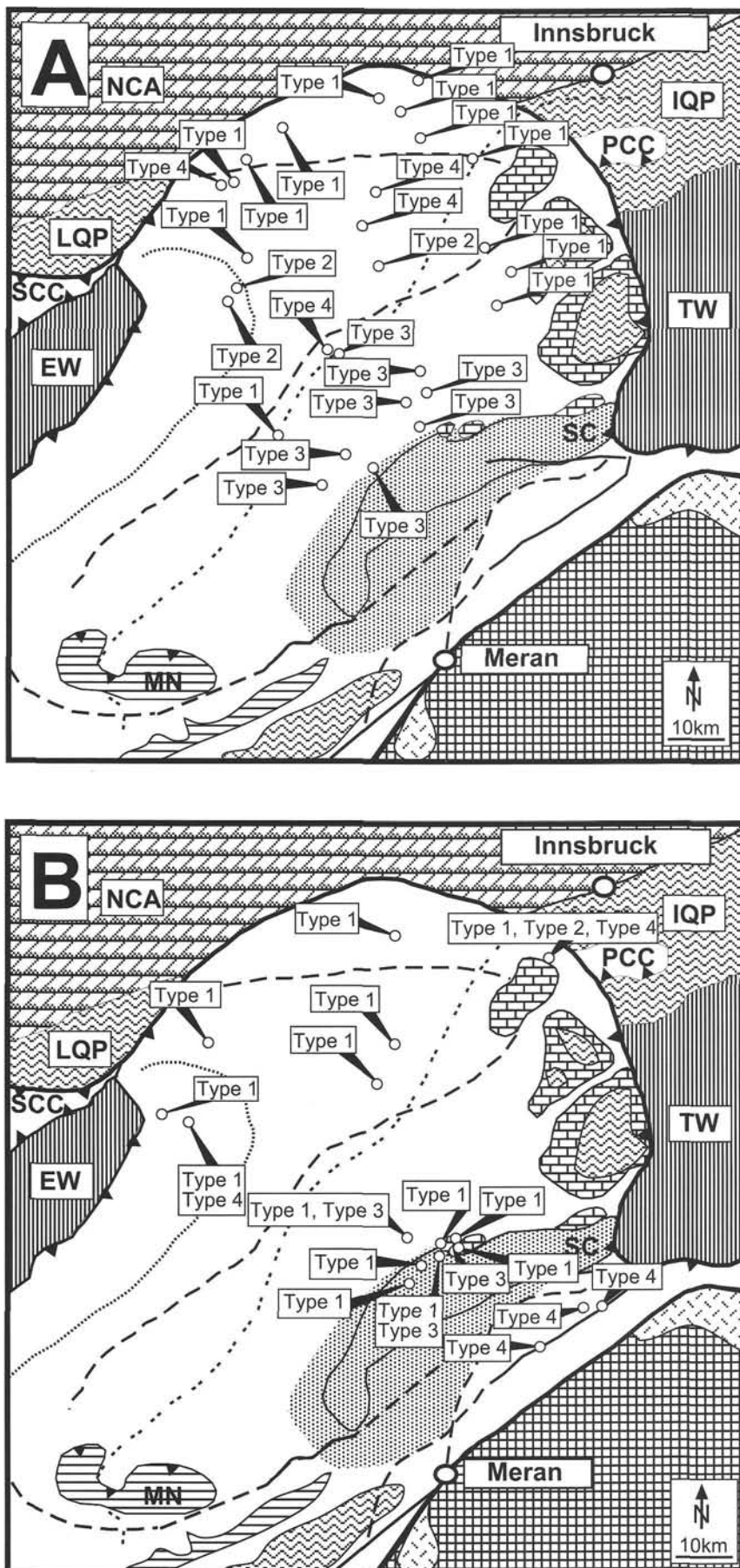
enrichment occurs in garnets from almost all samples (Fig. 4, Fig. 7A-D). Type 5 of VELTMAN (1986) actually belongs to Type 1 CaMn and Type 1 Mn according to the classification scheme used in this study. Garnet rims, enriched in Mn have been attributed to either diffusion (e. g. SPEAR, 1993), breakdown reactions of Mn-rich phases such as ilmenite or resorption of garnet involving adjacent biotite along the retrograde portion of the P-T path. Since biotite is low in Mn and shows a lower $Fe^{2+}/(Fe^{2+}+Mg)$ ratio than garnet, adjacent garnet rims will start to deplete in Mg and therefore enrich in Fe^{2+} and Mn, which can clearly be seen in the outermost rims of the investigated samples (Fig. 7A, C, D). Diffusional processes only seem to involve the outermost $10\,\mu m$ of the garnet rims, since the rims in Figure 7A-D show a Mn-enrichment which is coeval with a decrease in Ca and Mg, which indicates that reactions after the thermal peak, involving the grossular and pyrope component, also simultanously take place. The Mn-enrichment also shows a positive correlation with the size of the garnet: the smaller the garnet, the greater the depth of the Mn-enrichment. This ranges from ca. 50 μm in garnets with diameters of >2000 μm (Fig. 7A, B) to ca. 100 μm in garnets with diameters of 500-700 μm (Fig. 7C, D). The Mn-enrichment also seems to be stronger in the western part of the ÖC where the Eo-Alpine metamorphic overprint is almost lacking and decreases towards the areas which show a strong amphibolite-facies Eo-Alpine overprint (Fig. 4).

Staurolite: Some staurolites show a continuous chemical zoning with cores that are slightly enriched in

Fig. 6
Regional distribution of the garnet zoning types from the investigations of (A) RECHEIS (1998) and (B) VELTMAN (1986). Originally, VELTMAN (1986) had slightly different types of garnet zoning than RECHEIS (1998). The garnet zoning types used in these Figures are discussed in the text and the garnet zoning types of RECHEIS (1998) were used in both Figures for clarity and to be able to compare the results. Legend is the same as in Figure 1A.
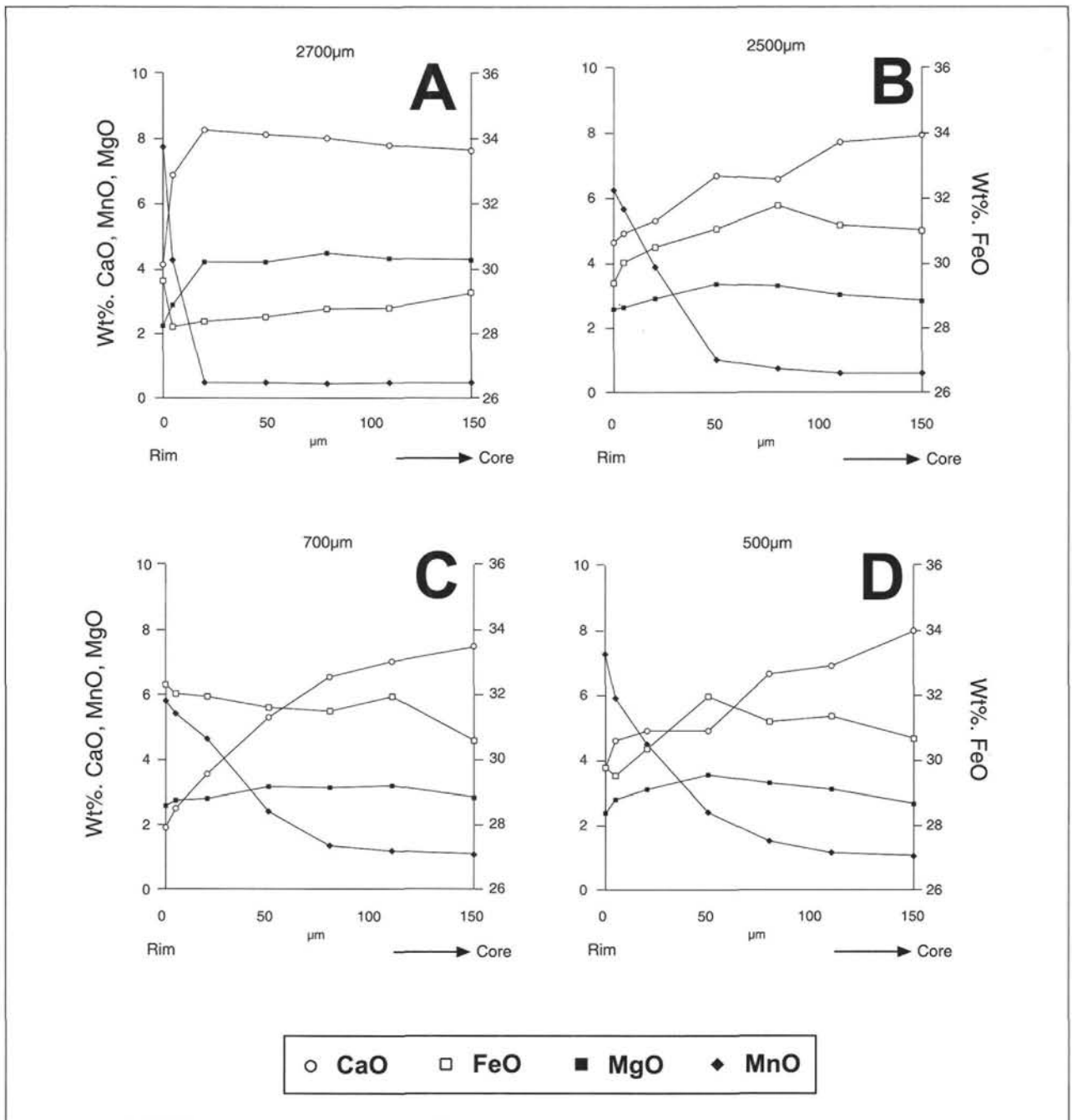
Fig. 7
Example illustrating the various depths of the Mn-enrichment in the outermost rims of the garnets depending on the size of the garnet: (A) 2700 μm, (B) 2500 μm, (C) 700 μm and (D) 500 μm.

Fe^{2+} (Table 4). The Mg content decreases and the Zn content increases towards the rims. Some of the staurolite rims have significant MnO and ZnO contents of 0.2-0.4 and 0.2-1.6 wt % respectively (Table 4). All staurolites are rich in Fe^{2+} and the Fe number [Fe^{2+}/(Fe^{2+}+Mg)] varies between 0.81 and 0.88. Sample Ö-447 contains staurolite as inclusions in garnet as well as matrix staurolite. The matrix staurolite show higher Mg and Zn contents and slightly lower Fe^{2+} contents. *Plagioclase* overgrows in most samples the main foliation and these texturally late growing porphyroblasts are chemically homogeneous (An$_{30-35}$). Overall, the anorthite content of the samples varies between An$_{10}$ and

An$_{30}$ (Table 5). In a few samples (2-91; 79-11) small grains of inversely zoned plagioclase have been found with albite-rich cores (An$_{16-23}$) and increasing anorthite content towards the rim (An$_{27-30}$). Some plagioclase porphyroblasts show an increase of the albite content in the outermost rims (An$_{17-20}$) and these albite-rich rims are probably due to retrograde reactions. *Biotite*: All biotites are unzoned and rich in FeO (16-22 wt %). TiO$_2$ is low and varies between 1.36 and 2.67 wt % (Table 6). *Muscovite* occurs together with biotite oriented in the planes of schistosity. The Si content is 2.96-3.25 Si apfu and the paragonite content is 10-20 mol % (Table 7).

Table 4
Representative microprobe analyses of staurolite.

Sample	80-15 core	80-15 rim	Ö-526 core	Ö-526 rim	Ö-492 core	Ö-492 rim	80-20 core	80-20 rim	Ö-447 matrix	Ö-447 incl. in grt	80-3 core
SiO_2	28.05	28.14	27.27	27.49	26.88	27.00	27.80	27.66	26.62	27.74	28.27
TiO_2	0.63	0.84	0.60	0.55	0.72	0.62	0.74	0.56	0.51	0.48	0.70
Al_2O_3	54.93	54.90	53.97	53.25	52.68	53.82	54.46	55.51	53.84	53.26	55.51
FeO	12.05	11.58	14.40	13.81	14.89	15.14	13.52	13.72	14.54	15.04	11.53
MnO	0.16	0.40	0.09	0.26	0.25	0.34	0.35	0.18	0.24	0.20	0.38
MgO	1.27	0.91	1.45	1.28	1.32	1.32	1.77	1.13	1.61	1.09	1.21
ZnO	0.52	1.06	n.d.	0.22	0.05	0.73	n.d.	n.d.	0.54	0.05	1.56
CaO	n.d.	n.d.	n.d.	0.07	0.01	0.05	n.d.	0.04	n.d.	0.06	n.d.
NiO	0.06	0.15	n.d.	0.07	0.04	n.d.	n.d.	n.d.	0.06	n.d.	n.d.
Na_2O	0.20	0.20	0.18	n.d.	0.07	n.d.	0.03	n.d.	n.d.	0.05	0.28
K_2O	0.08	0.02	n.d.	0.02	0.07	n.d.	0.02	n.d.	0.01	n.d.	0.05
Total	97.96	98.31	98.00	97.30	96.98	99.02	98.69	98.93	97.97	98.01	99.59
Si	7.729	7.741	7.587	7.699	7.595	7.501	7.645	7.583	7.449	7.737	7.692
Al(IV)	0.271	0.259	0.413	0.301	0.405	0.499	0.355	0.417	0.551	0.263	0.308
Al(VI)	17.566	17.54	17.283	17.274	17.138	17.122	17.296	17.517	17.203	17.244	17.492
Ti	0.130	0.174	0.125	0.116	0.153	0.129	0.153	0.115	0.107	0.101	0.143
Fe^{2+}	2.776	2.663	3.359	3.234	3.518	3.517	3.109	3.145	3.402	3.507	2.623
Mn	0.037	0.093	0.021	0.061	0.059	0.080	0.082	0.042	0.057	0.047	0.087
Mg	0.521	0.374	0.601	0.534	0.556	0.547	0.725	0.462	0.672	0.453	0.490
Zn	0.106	0.216	n.d.	0.045	0.010	0.149	n.d.	n.d.	0.112	0.010	0.313
Ca	n.d.	n.d.	n.d.	0.021	0.003	0.015	n.d.	0.012	n.d.	0.018	n.d.
Ni	0.013	0.033	n.d.	0.016	0.009	n.d.	n.d.	n.d.	0.013	n.d.	n.d.
Na	0.108	0.107	0.097	n.d.	0.039	n.d.	0.016	n.d.	n.d.	0.027	0.147
K	0.028	0.007	n.d.	0.007	0.026	n.d.	0.007	n.d.	0.003	n.d.	0.018
ΣCations	29.288	29.231	29.487	29.370	15.65	29.559	29.388	29.321	29.569	29.416	29.335

Basis of formula calculation: 46 oxygens; n.d. not detected

Table 5
Representative microprobe analyses of plagioclase.

Sample	2-91 core	2-91 rim	79-11 core	79-11 rim	91-3	Ö-492	80-3	80-77	74-1	P-8b	75-2
SiO_2	64.84	60.78	62.08	60.56	62.60	64.65	60.97	62.03	63.03	59.35	63.56
TiO_2	n.d.	n.d.	n.d.	n.d.	n.d.	n.d.	n.d.	n.d.	n.d.	0.02	n.d.
Al_2O_3	23.47	25.15	24.06	25.66	22.87	23.07	24.42	24.37	22.78	25.71	23.06
Cr_2O_3	n.d.	n.d.	n.d.	n.d.	n.d.	n.d.	n.d.	n.d.	n.d.	n.d.	n.d.
[a]Fe_2O_3	0.04	0.09	0.26	0.13	0.06	0.09	0.04	0.82	0.19	0.66	0.02
MnO	0.02	0.01	0.03	n.d.	n.d.	0.02	n.d.	0.01	0.02	0.03	0.03
MgO	n.d.	0.01	n.d.	0.06	0.02	n.d.	n.d.	n.d.	0.01	0.01	n.d.
CaO	3.32	6.29	4.79	5.02	4.43	1.87	5.32	4.12	3.97	6.40	3.75
Na_2O	9.52	8.24	8.87	7.29	9.11	9.42	8.51	8.70	9.51	7.81	9.30
K_2O	0.16	0.10	0.14	0.05	0.08	0.09	0.10	0.09	0.11	0.11	0.12
Total	101.37	100.67	100.24	98.77	99.17	99.21	99.36	100.14	99.90	100.10	99.84
Si	2.817	2.687	2.746	2.703	2.792	2.851	2.722	2.742	2.874	2.649	2.809
Al	1.202	1.311	1.255	1.350	1.203	1.199	1.285	1.270	1.142	1.352	1.201
Ti	n.d.	n.d.	n.d.	n.d.	n.d.	n.d.	n.d.	n.d.	n.d.	0.001	n.d.
Cr	n.d.	n.d.	n.d.	n.d.	n.d.	n.d.	n.d.	n.d.	n.d.	n.d.	n.d.
[a]Fe^{3+}	0.001	0.003	0.009	0.004	0.002	0.003	0.001	0.027	0.005	0.025	0.001
Mn	0.001	n.d.	0.001	n.d.	n.d.	0.001	n.d.	n.d.	n.d.	0.001	0.001
Mg	n.d.	0.001	n.d.	0.004	0.001	n.d.	n.d.	n.d.	0.011	0.001	n.d.
Ca	0.155	0.298	0.227	0.240	0.212	0.088	0.254	0.195	0.109	0.306	0.177
Na	0.802	0.706	0.761	0.631	0.788	0.805	0.737	0.746	0.752	0.676	0.797
K	0.009	0.006	0.008	0.003	0.005	0.005	0.006	0.005	0.070	0.006	0.007
Σ Cations	4.987	5.012	5.006	4.936	5.002	4.953	5.006	4.985	4.965	5.015	4.993
Albite	0.83	0.69	0.76	0.72	0.78	0.89	0.74	0.79	0.81	0.68	0.81
Anorthite	0.16	0.30	0.23	0.27	0.21	0.10	0.25	0.20	0.18	0.31	0.18
Orthoclase	0.01	0.01	0.01	0.01	0.01	0.01	0.01	0.01	0.01	0.01	0.01

[a]Calculated; Basis of formula calculation 8 oxygens; n.d. not detected

Table 6
Representative microprobe analyses of biotite.

Sample	2-91	79-11	P-8b	91-3	Ö-492	80-15	80-3	Ö-526	75-2	80-77	74-3
SiO_2	35.45	37.41	32.90	35.44	33.05	37.53	36.35	35.09	35.04	34.64	36.15
TiO_2	1.56	1.46	2.67	1.87	1.69	1.60	1.77	1.52	2.00	1.90	1.36
Al_2O_3	19.19	20.04	16.94	18.94	20.51	18.88	18.39	19.38	18.63	19.49	18.77
Cr_2O_3	n.d.	n.d.	n.d.	0.24	0.05	0.06	n.d.	n.d.	n.d.	n.d.	n.d.
$^aFe_2O_3$	n.d.	n.d.	1.93	n.d.	3.71	n.d.	n.d.	1.81	n.d.	n.d.	1.14
FeO	20.10	16.94	18.47	18.73	18.90	17.63	18.64	19.85	22.38	21.36	16.35
MnO	0.12	0.04	0.75	0.29	0.08	0.04	0.17	0.11	0.01	0.06	0.39
MgO	9.97	11.65	9.69	9.73	8.73	10.13	9.66	9.67	8.00	7.71	11.72
CaO	0.03	0.01	0.03	n.d.	n.d.	n.d.	0.04	n.d.	n.d.	n.d.	0.08
Na_2O	0.08	0.41	0.10	0.22	0.14	0.30	0.38	0.23	0.46	0.39	0.28
K_2O	9.55	8.26	9.19	8.49	8.53	8.89	8.72	9.15	8.91	8.75	8.50
Total	96.11	96.23	92.70	93.96	95.40	95.07	94.13	96.82	95.44	94.31	94.74
Si	2.685	2.749	2.613	2.716	2.531	2.813	2.777	2.645	2.699	2.684	2.722
Al(IV)	1.315	1.251	1.387	1.284	1.469	1.187	1.223	1.355	1.301	1.316	1.278
Al(VI)	0.399	0.485	0.199	0.427	0.383	0.481	0.433	0.367	0.391	0.464	0.388
Ti	0.089	0.081	0.159	0.108	0.097	0.090	0.102	0.086	0.116	0.111	0.077
Cr	n.d.	n.d.	n.d.	0.015	0.003	0.004	n.d.	n.d.	n.d.	n.d.	n.d.
$^aFe^{3+}$	n.d.	n.d.	0.116	n.d.	0.214	n.d.	n.d.	0.103	n.d.	n.d.	0.064
Fe^{2+}	1.273	1.041	1.227	1.201	1.211	1.105	1.191	1.251	1.442	1.384	1.030
Mn	0.008	0.002	0.050	0.019	0.005	0.003	0.011	0.007	0.001	0.004	0.025
Mg	1.125	1.276	1.147	1.111	0.996	1.131	1.100	1.086	0.918	0.890	1.315
Ca	0.002	0.001	0.003	n.d.	n.d.	n.d.	0.003	n.d.	n.d.	n.d.	0.006
Na	0.012	0.058	0.015	0.033	0.021	0.044	0.056	0.034	0.069	0.059	0.041
K	0.924	0.775	0.932	0.831	0.834	0.851	0.851	0.881	0.876	0.866	0.817
ΣCations	7.835	7.719	7.85	7.745	7.765	7.708	7.747	7.814	7.812	7.777	7.765

^{a}Calculated; Basis of formula calculation11 oxygens; n.d. not detected

Table 7
Representative microprobe analyses of muscovite.

Sample	2-91	79-11	P-8b	91-3	Ö-492	80-15	80-3	Ö-526	75-2	80-77	74-3
SiO_2	45.59	44.20	45.26	47.47	44.45	46.40	48.11	46.07	47.15	47.80	49.04
TiO_2	0.45	0.49	0.64	0.56	0.55	0.77	0.76	0.60	0.62	0.44	0.67
Al_2O_3	37.47	36.62	31.91	34.68	39.64	36.02	34.09	35.76	31.18	36.92	31.86
Cr_2O_3	n.d.	0.03	n.d.	n.d.	0.09	0.21	0.02	0.15	0.04	n.d.	n.d.
$^{a}Fe_2O_3$	0.91	0.97	1.42	n.d.	0.76	0.54	n.d.	0.42	n.d.	n.d.	1.30
FeO	0.35	0.38	3.06	1.09	0.29	0.37	1.16	0.96	2.34	0.82	0.50
MnO	0.01	0.01	0.06	n.d.	0.02	n.d.	0.03	0.02	n.d.	n.d.	0.08
MgO	0.70	1.17	1.05	0.50	0.46	0.74	0.86	0.77	1.87	0.38	2.18
CaO	n.d.	0.02	n.d.	n.d.	n.d.	0.18	0.02	0.06	n.d.	0.01	n.d.
Na_2O	0.81	1.36	0.63	1.94	1.28	1.06	1.14	1.60	0.62	1.01	0.76
K_2O	9.64	8.89	10.66	8.31	8.37	7.97	9.23	7.98	10.32	8.32	7.54
Total	95.94	94.15	94.70	94.56	95.92	94.26	95.43	94.40	94.15	95.71	93.94
Si	2.995	2.963	3.090	3.146	2.905	3.070	3.170	3.060	3.195	3.109	3.246
Al(IV)	1.005	1.027	0.910	0.854	1.095	0.930	0.830	0.940	0.815	0.891	0.754
Al(VI)	1.897	1.867	1.659	1.856	1.959	1.880	1.818	1.860	1.676	1.940	1.732
Ti	0.022	0.025	0.033	0.028	0.027	0.038	0.038	0.030	0.032	0.022	0.033
Cr	n.d.	0.002	n.d.	n.d.	0.005	0.011	0.001	0.008	0.002	n.d.	n.d.
$^{a}Fe^{3+}$	0.045	0.049	0.073	n.d.	0.037	0.027	n.d.	0.021	n.d.	n.d.	0.065
Fe^{2+}	0.019	0.021	0.175	0.060	0.016	0.020	0.064	0.054	0.133	0.045	0.028
Mn	0.001	0.001	0.003	n.d.	0.001	n.d.	0.002	0.001	n.d.	n.d.	0.004
Mg	0.069	0.117	0.107	0.049	0.045	0.073	0.084	0.076	0.189	0.037	0.215
Ca	n.d.	0.001	n.d.	n.d.	n.d.	0.013	0.001	0.004	n.d.	0.001	n.d.
Na	0.103	0.177	0.083	0.249	0.162	0.136	0.146	0.206	0.081	0.127	0.098
K	0.809	0.761	0.929	0.703	0.699	0.674	0.777	0.677	0.893	0.691	0.637
ΣCations	6.965	7.009	7.063	6.947	6.951	6.872	6.930	6.937	7.015	6.893	6.813

^{a}Calculated; Basis of formula calculation 11 oxygens; n.d. not detected

5. Thermobarometry

5.1 Application of conventional geothermometry

Cation exchange and net transfer reactions are well established as geothermometers and geobarometers (ESS-ENE, 1982, 1989). The equations for temperature and pressure calculation are mainly based on experimental results of either synthetic or natural mineral phases. Activity models have to be applied to take non ideal mixing behavior into account. The disadvantage is that the equilibria are not calculated from a single consistent data set but rather from different and inconsistent sources. The garnet-biotite thermometer was applied to different areas within a thin section, to demonstrate the influence of polymetamorphism on the temperature results. The modal amount of muscovite in the samples is low and they fulfill the thermobarometric requirement of high modal proportions of plagioclase and biotite over garnet. This allows the assumption of an infinite reservoir concept and prevents large compositional modifications in the mineral phases during the retrograde P-T path and makes it also possible to obtain data from portions all over the thin section (SPEAR et al., 1991b, SPEAR 1993).

Cation exchange thermometers between garnet and biotite were applied using the calibration of FERRY and SPEAR (1978) with the garnet model of BERMAN (1990). HOINKES (1986b) used garnets from the SC to demonstrate the effect of X_{Grs} on this thermometer. Because of the garnet zonation only coexisting garnet-biotite pairs have been used. Due to the polymetamorphic nature of the samples from the ÖC, chemical variations occur, which mainly affect the Fe^{2+}/Mg ratio of the garnet rims (TROPPER and HOINKES, 1996). This leads to a large variation of temperatures within sample

Ö-336 of nearly 100°C between 450-550°C. Overall, the *garnte-biotite temperatures lie in most samples* (91-3, 80-75, 80-77, Ö-447, P8, Ö-492) within 450-660°C.

The garnets in the selected samples show continuous zoning profiles and narrow retrograde rims (ca. 30 μm) which show an increase in MnO and a decrease in MgO. The depth of the enrichment ranges from 40 μm to >100 μm (Figs. 7A-D). The depth of the MnO-enrichment varies within the area of investigation. In the western part of the ÖC, the depth of the enrichment is very large and decreases towards the area of the Eo-Alpine garnet formation. The increase of MnO in the outermost rims usually leads to a decrease of MgO and therefore a decrease in the obtained temperatures. In the samples of this investigation the increase in MnO is associated either with (1.) a continuous a decrease of FeO and MgO but constant CaO (sample Ö-492) as shown in Figure 8A or (2.) a continuous decrease of CaO, MgO and FeO (sample P-8) as shown in Figure 8B. Taking garnet rim analyses from the first case will yield temperatures related to the growth of the garnets since CaO is constant, but in the second case these temperatures represent only temperatures of a later retrograde stage since CaO also decreases. In the first case rim temperatures of samples 91-3 and P8 yield 580-640°C. Therefore temperatures obtained with the lowest MnO and the highest MgO, correlated with prograde zoning in garnet may be interpreted as being close to the maximum temperatures. Samples where garnets were modified by diffusion yield temperatures of 470-520°C (80-77, Ö-447, Ö-492). Calculating the temperatures with the lowest MnO and the highest MgO, raises the temperatures to 600-660°C which is interpreted as the peak temperatures.
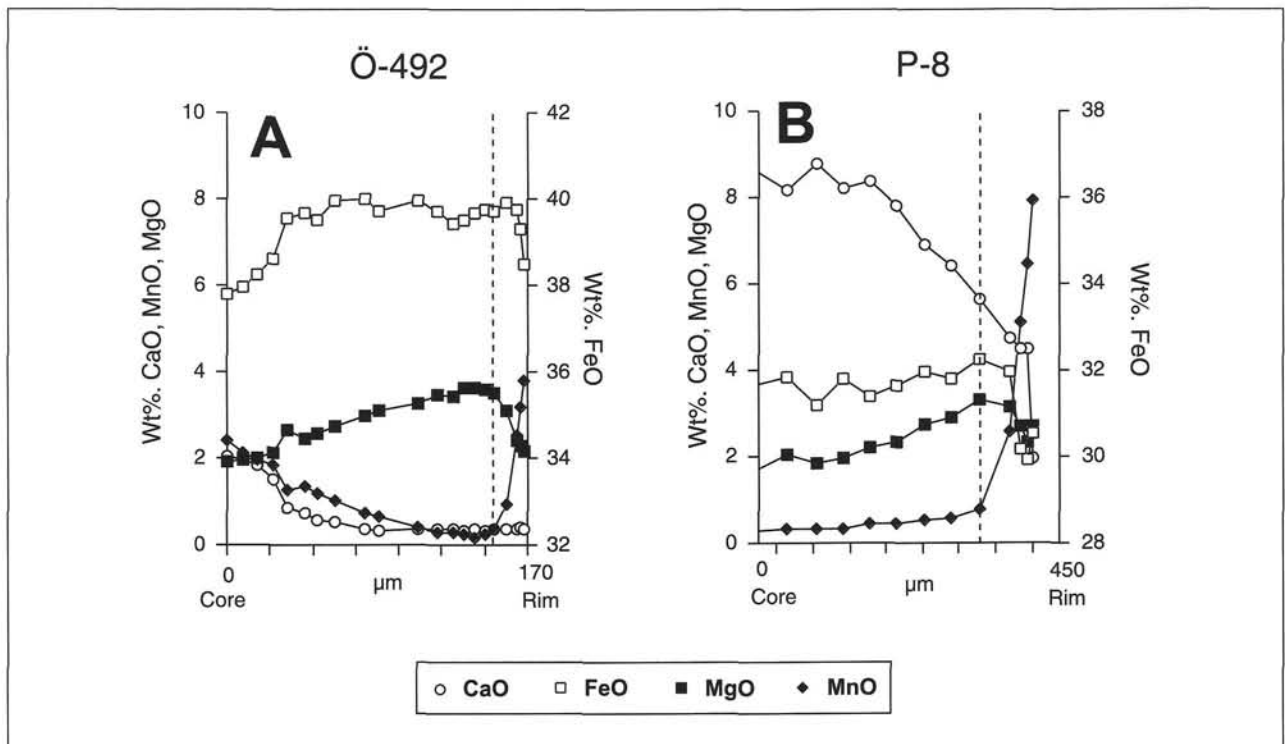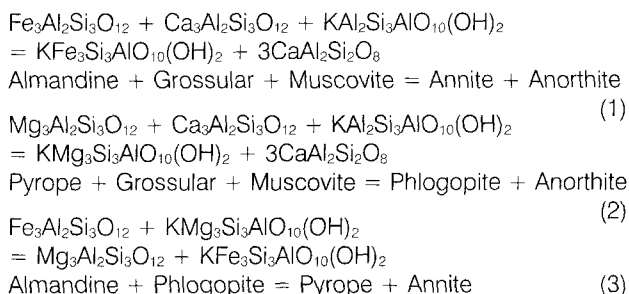

Fig. 8
The increase of MnO in the outermost rims usually leads to a decrease of MgO and therefore a decrease in the obtained temperatures. The increase in MnO is associated either with (A) a continuous a decrease of FeO and MgO but constant CaO (sample Ö-492) or (B) a continuous decrease of Ca, Mg and Fe (sample P-8).

5.2 Application of multi-equilibrium calculations

The simultaneous calculation of all possible reactions within a defined chemical system has been done by using the program THERMOCALC v. 2.7 (HOLLAND, 1999, written comm.) and the data set of HOLLAND and POWELL (1998). The natural composition of coexisting minerals is taken into account using the activity models for garnet, plagioclase, muscovite and biotite from the set of proposed activity models from the program MacAX (HOLLAND, 1999, written comm.). Since no reliable data on staurolite solid solutions are available, it has been omitted from the calculations. Activities of Al_2SiO_5 and SiO_2 are taken as 1. To avoid uncertainties due to poor knowledge of H_2O activity, in a first attempt only H_2O-absent reactions are taken into account to calculate an H_2O-absent intersection. The activities were calculated at 6 kbar and 600 °C, to calculate the intersections and the P-T conditions of the intersections. Subsequently the determined conditions were used to re-calculate the activities again. This iteration process was repeated until the data converged to less than 0.1 kbar and 10 °C. These conditions are used subsequently to estimate $a(H_2O)$ by calculating P-$a(H_2O)$ diagrams. These calculations have mostly been performed on samples, rich in plagioclase and biotite, except sample 80-20 which does not contain plagioclase.

For samples containing the assemblage garnet + biotite + plagioclase + muscovite + quartz three reactions were used to derive the P-T conditions of the equilibrium assemblage during garnet rim formation:

$Fe_3Al_2Si_3O_{12}$ + $Ca_3Al_2Si_3O_{12}$ + $KAl_2Si_3AlO_{10}(OH)_2$
= $KFe_3Si_3AlO_{10}(OH)_2$ + $3CaAl_2Si_2O_8$
Almandine + Grossular + Muscovite = Annite + Anorthite   (1)

$Mg_3Al_2Si_3O_{12}$ + $Ca_3Al_2Si_3O_{12}$ + $KAl_2Si_3AlO_{10}(OH)_2$
= $KMg_3Si_3AlO_{10}(OH)_2$ + $3CaAl_2Si_2O_8$
Pyrope + Grossular + Muscovite = Phlogopite + Anorthite   (2)

$Fe_3Al_2Si_3O_{12}$ + $KMg_3Si_3AlO_{10}(OH)_2$
= $Mg_3Al_2Si_3O_{12}$ + $KFe_3Si_3AlO_{10}(OH)_2$
Almandine + Phlogopite = Pyrope + Annite   (3)

Reactions (1) and (2) are the Fe- and Mg-end-member reactions between the phases garnet, plagioclase, muscovite and biotite. Reaction (3) is the garnet-biotite thermometer. These reactions intersect in intersection (I).

For samples containing the assemblage garnet + kyanite + biotite + plagioclase + muscovite + quartz the following reactions, intersecting in two H_2O-absent intersections (II, III), were used:

The second intersection (II) is constrained with the reactions:

Table 8
Results of the multi-equilibrium P-T calculations with THERMOCALC v. 2.7.

Sample	Intersection I				Intersection II				Intersection III				$a(H_2O)$	Unit
	P	σ	T	σ	P	σ	T	σ	P	σ	T	σ		
2-91	4.2	0.9	469	56									0.32	ÖC
79-11	8.8	1.1	556	65									-	ÖC
P-8b	6.9	1.3	637	89									>1.0	ÖC
Ö-492	5.6	1.2	644	83									0.65	ÖC
Ö-526	5.7	1.1	621	75									0.81	ÖC
75-2	8.6	1.4	669	86									>1.0	ÖC
91-3	7.3	1.2	630	75									-	ÖC
80-77	6.0	1.2	705	90	6.0	1.2	708	79	6.2	2.7	706	84	>1.0	ÖC
74-3	7.2	1.0	578	66	7.3	1.0	586	54	7.8	2.8	580	60	0.42	ÖC
Ö-447	8.3	1.2	644	75	8.3	1.1	650	62	8.6	2.8	646	68	0.98	ÖC
80-15	6.1	1.0	543	63	6.3	1.0	566	55	7.7	1.0	543	66	0.50	MMB
80-3	5.9	1.0	562	67	5.9	1.0	558	57	5.6	2.6	561	62	0.63	MMB
80-20									5.3	2.5	644	75	-	MMB
79-3	9.8	1.3	574	68									0.19	SC
74-28	9.3	1.2	551	64									0.26	PC

ÖC: Ötztal Complex,; SC: Scneeberg Complex; PC: Permoscythian cover sequence; P: kbar; T: °C; σ: 1 σ standard deviation; invariant points (I) - (III) are listed in the text.
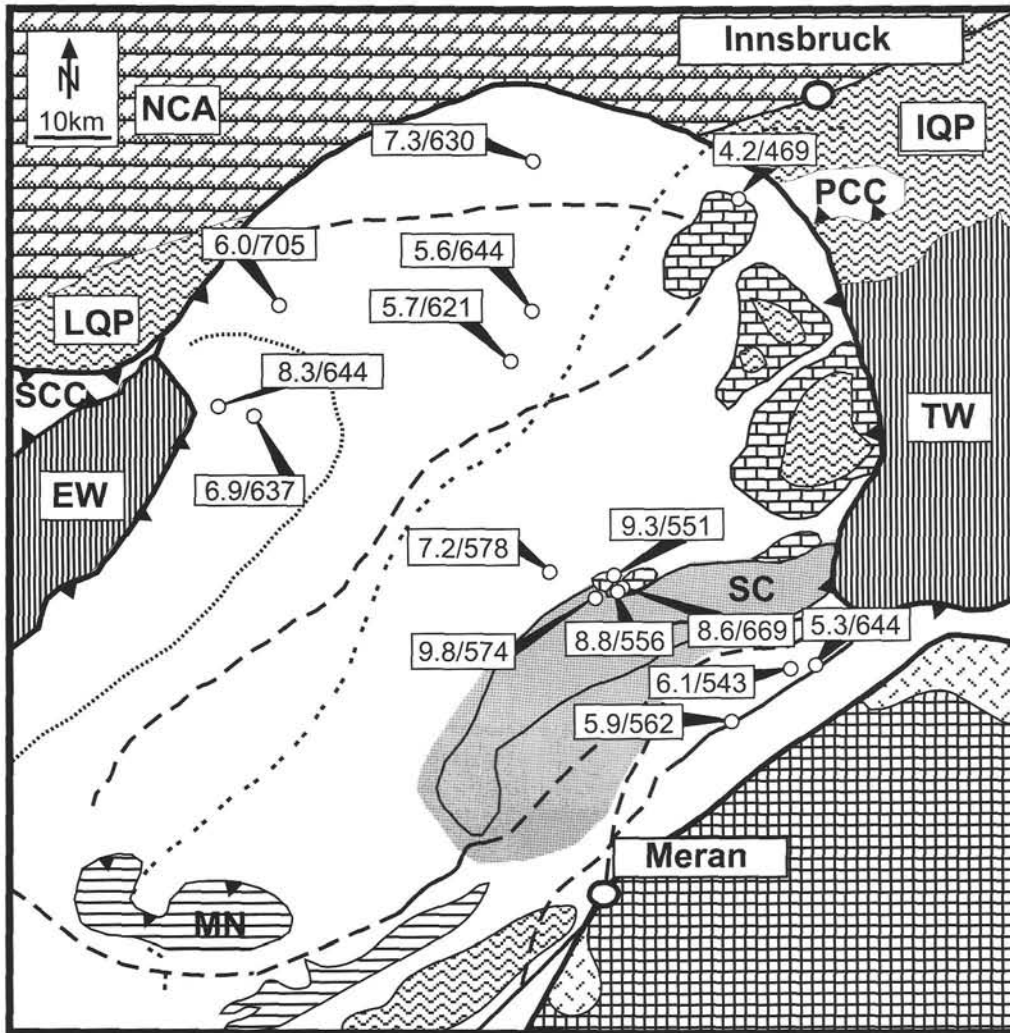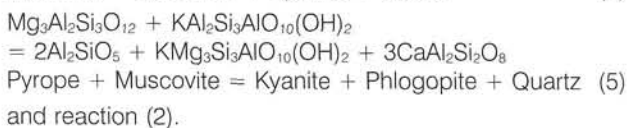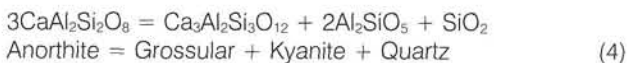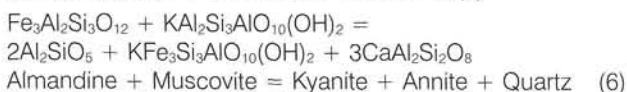
Fig. 9
Regional distribution of the results of the multi-equilibrium calculations with THERMOCALC v. 2.7 (HOLLAND, 1999, written comm.). The grey rectangles show the Variscan P-T results and the white rectangles show the Eo-Alpine P-T results. Legend is the same as in Figure 1A.
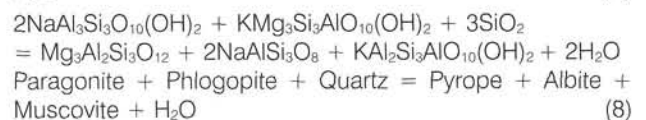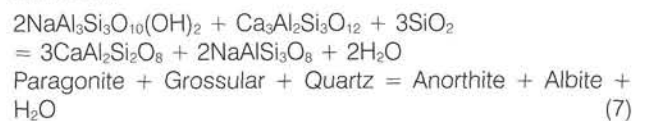
from the Meran-Mauls Basement (MMB) are very similar and range from 543°C and 5.9 kbar (sample 80-3) to 644°C and 5.3 kbar (sample 80-20). The Eo-Alpine P-T conditions obtained from the ÖC range from 469°C and 4.2 kbar (sample 2-91) in the north underneath the Permoscythian Kalk-kögel to 556°C and 8.8 kbar (sample 79-11) in the south close to the SC. The highest Eo-Alpine pressures were obtained from the samples of the SC and PC with 9.3-9.8 kbar at 551-574°C (Fig. 9). The standard deviation for all calculations in Table 8 is 1σ.

Adding H_2O to the calculations allows to calculate P-log $a(H_2O)$-diagrams. These calculations were only possible by extending the system to NKF-MASH, by adding paragonite and albite. The calculation of $a(H_2O)$ was performed for kyanite-free samples with intersections involving the phases garnet, biotite, plagioclase, muscovite and quartz involving reactions (1), (2) and the reactions:

$2NaAl_3Si_3O_{10}(OH)_2 + Ca_3Al_2Si_3O_{12} + 3SiO_2$
$= 3CaAl_2Si_2O_8 + 2NaAlSi_3O_8 + 2H_2O$
Paragonite + Grossular + Quartz = Anorthite + Albite + H_2O (7)

$2NaAl_3Si_3O_{10}(OH)_2 + KMg_3Si_3AlO_{10}(OH)_2 + 3SiO_2$
$= Mg_3Al_2Si_3O_{12} + 2NaAlSi_3O_8 + KAl_2Si_3AlO_{10}(OH)_2 + 2H_2O$
Paragonite + Phlogopite + Quartz = Pyrope + Albite + Muscovite + H_2O (8)

For kyanite-bearing samples, intersections involving reactions (4), (5), (7) and the paragonite-out reaction

$NaAl_3Si_3O_{10}(OH)_2 + SiO_2 = NaAlSi_3O_8 + Al_2SiO_5 + H_2O$
Paragonite + Quartz = Albite + Kyanite + H_2O (9)
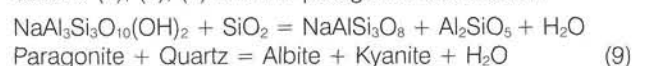
were calculated. Due to the lack of paragonite or albite, $a(H_2O)$ could not be calculated in three samples (79-11, 91-3, 80-20). The calculations yield $a(H_2O)$, ranging from 0.19 to 0.98 and hence lower than 1.0 for most samples, thus indicating the dilution of the presumably H_2O-bearing

$3CaAl_2Si_2O_8 = Ca_3Al_2Si_3O_{12} + 2Al_2SiO_5 + SiO_2$
Anorthite = Grossular + Kyanite + Quartz   (4)

$Mg_3Al_2Si_3O_{12} + KAl_2Si_3AlO_{10}(OH)_2$
$= 2Al_2SiO_5 + KMg_3Si_3AlO_{10}(OH)_2 + 3CaAl_2Si_2O_8$
Pyrope + Muscovite = Kyanite + Phlogopite + Quartz   (5)

and reaction (2).

The third intersection (III) is constrained with the reactions (3), (5) and the Fe-endmember reaction of (5)

$Fe_3Al_2Si_3O_{12} + KAl_2Si_3AlO_{10}(OH)_2 =$
$2Al_2SiO_5 + KFe_3Si_3AlO_{10}(OH)_2 + 3CaAl_2Si_2O_8$
Almandine + Muscovite = Kyanite + Annite + Quartz   (6)

Calculations of the Variscan P-T conditions of ÖC samples, containing the metapelite assemblage: garnet (rim) – biotite – plagioclase – muscovite – quartz (intersection I in the KFMASH system), yield P-T results ranging from 621°C and 5.7 kbar (sample Ö-526) to 705°C and 6.0 kbar (sample 80-77) as shown in Table 8 and Figure 9. Calculations of P and T from samples containing kyanite as an additional phase, result in P-T conditions, similar to the conditions mentioned before (Table 8). The Variscan P-T conditions

fluid by other components (e. g. CO_2 or NaCl). This is in accordance with fluid inclusion studies by KAINDL et al. (1999) which showed the presence of NaCl in primary fluid inclusions from garnets from the southern Kaunertal area in the northwest of the ÖC. Three samples yielded $a(H_2O)$ >1.0, which resulted from considerable shift in the paragonite activity, thus indicating problems with the thermodynamic model of paragonite used in the calculations (Table 8).

5.3 Application of the inverse equilibrium approach

Most thermobarometric methods begin with measurements of the compositions of coexisting mineral solid solutions, from which the thermodynamic activities of the endmembers of the solid solutions can be determined. These values are then substituted into the equations describing the free energy changes among the end-members and to solve these equations for pressure and temperature. This web-based approach also called WEBINVEQ uses a different approach which is called the inverse chemical equilibrium problem (GORDON, 1998). In this approach, by giving the activities of the end-members of the coexisting minerals, a least squares estimate of the pressure and temperature of the equilibration of a mineral assemblage is calculated, based on the activities of the participating phases.

Table 9
Results of the P-T calculations using WEBINVEQ.

Sample	P	σ	T	σ	Unit
2-91	3.7	0.6	485	25	ÖC
79-11	8.3	0.6	547	25	ÖC
P-8b	6.9	0.7	648	30	ÖC
Ö-492	6.3	0.6	708	32	ÖC
Ö-526	6.3	0.6	663	31	ÖC
75-2	8.6	0.7	687	29	ÖC
91-3	6.8	0.6	638	30	ÖC
80-77	5.7	0.6	691	29	ÖC
74-3	7.5	0.6	620	26	ÖC
Ö-447	8.1	0.7	651	27	ÖC
80-15	5.8	0.6	569	25	MMB
80-3	5.4	0.6	569	26	MMB
79-3	10.4	0.7	608	27	SC
74-28	10.1	0.7	576	27	PC

ÖC: Ötztal Complex; MMB: Meran-Mauls Basement; SC: Scneeberg Complex; PC: Permoscythian cover sequence; P: kbar; T: °C; σ: 1 σ standard deviation.

Instead of using a set of independent equilibria, P and T estimates are found by finding the best-fit hyperplane to the partial molar free energies of all phase components. The basic principles of the method are described by GORDON (1992). For the samples of the ÖC, this methods yields similar results as the multi-equilibrium calculations with Variscan P-T conditions of 638-708 °C and 5.7-8.1 kbar. In the MMB, the Variscan P-T results are very similar with temperatures of 569 °C and 5.4-5.8 kbar. The Eo-Alpine P-T conditions of 485-687 °C and 8.3-8.6 kbar (Table 9, Figures 10A, B). The highest pressures were obtained from the SC and PC with 10.1-10.4 kbar.

5.4 Change of P-T conditions during garnet growth

In a metamorphic system mineral composition is a function of pressure and temperature and therefore it is possible to model pressure and temperature by using mass balance considerations within a mineral assemblage and compositional variables. The calculation requires the compositions and modal proportions of the mineral assemblage and a starting condition, which has been obtained by thermobarometry (SPEAR, 1993). The computer software GIBBS (SPEAR et al., 1991a) has been applied to six samples with variably zoned garnets. The obtained thermobarometric estimates for garnet rim compositions range from 469 °C and 4.2 kbar to 630 °C and 7.3 kbar and were used as starting conditions. The P-T path has been modeled with the compositions of the garnets by using X_{Alm}-X_{Gro}, X_{Alm}-X_{Spe} and X_{Sps}-X_{Gro} pairs as compositional variables. The contrasting results show no definitive answer. In most samples (Ö-492, Ö-526, 91-3), pressure increases with decreasing temperature in the first steps of the calculated path. Afterwards no general trend could be found. In addition two samples show an increase in pressure with temperature (2-91, P-8b), which is contrary to the results obtained by VELTMAN (1986), TROPPER and HOINKES (1996) and PERGHER (1997). Sample 80-77 shows a decrease in pressure with a decrease in temperature, followed by a strong increase in pressure again. TROPPER and HOINKES (1996) and PERGHER (1997) also applied this method to Mn-enriched rims and also found an increase in pressure accompanied with a decrease in temperature. Applying this method to the outermost rims of our samples yielded no answer at all! Since there is no information on the equilibrium assemblage during garnet growth because of the lack of inclusion assemblages the quantitative information obtained from these calculations must be considered with caution.

6. Discussion

This investigation represents a continuation of the investigations of VELTMAN (1986) who started to study the regional variation of garnet zoning types within the ÖC (Figs. 6B, 11). The continuously zoned garnets of Type 1 occur within the whole ÖC, PC and SC where the most common zoning type is Type 1 MnCa (Figs. 6A, B, 11, Table 2). In contrast SPIESS et al. (2000) report discontinuously zoned garnets from the western ÖC which they interpret as a temporally stop of garnet growth due to stepping out and subsequent re-entering of garnet-forming P-T fields during
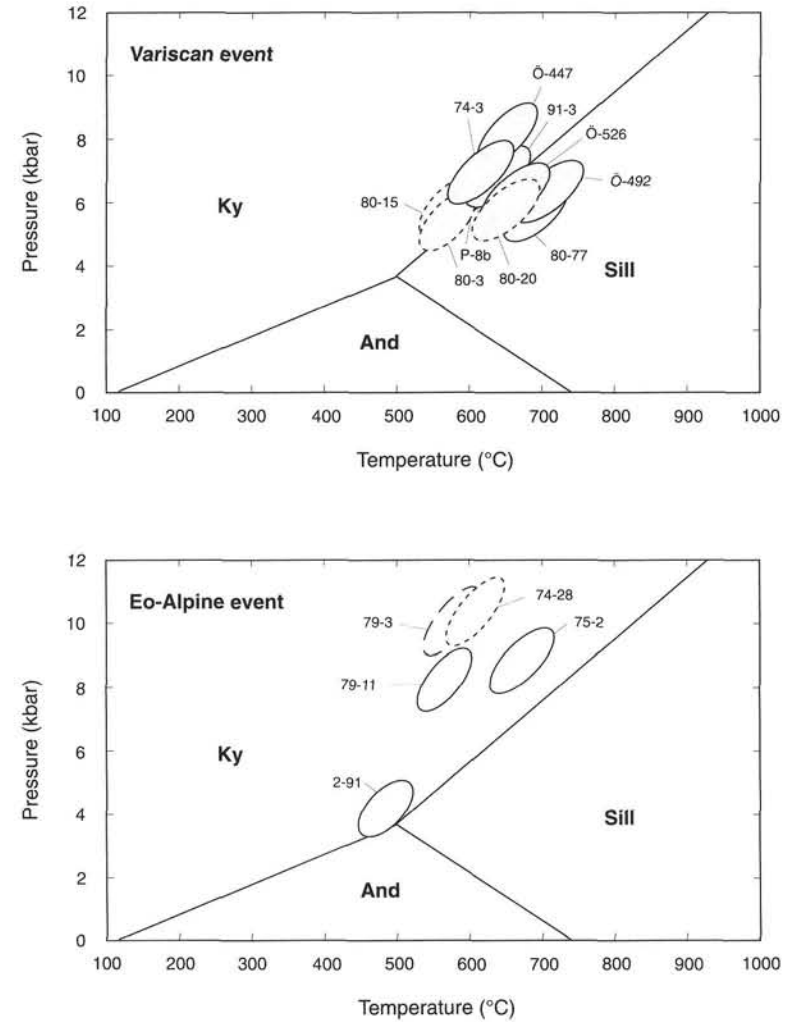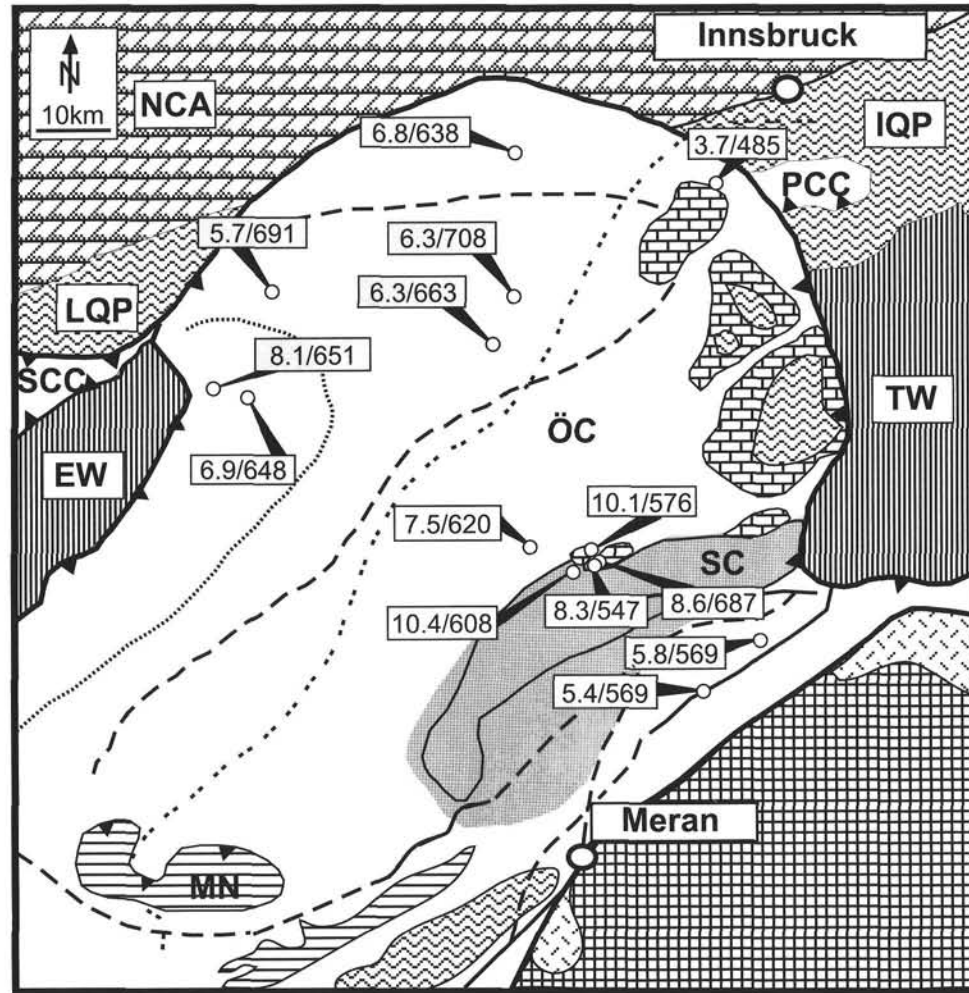
Fig. 10
Results of the WEBINVEQ calculations (GORDON, 1992).
A. Regional distribution of the results of the WEBINVEQ calculations. The grey rectangles show the Variscan P-T results and the white rectangles show the Eo-Alpine P-T results. Legend is the same as in Figure 1A.
B. P-T diagrams illustrating the thermobarometric estimates and the error ellipses of the Variscan and Eo-Alpine metamorphic events. The results of the Variscan event are shown as grey ellipses and are from the ÖC and the Meran-Mauls Basement (MMB). The data from the MMB are shown as stippled ellipses. The results for the Eo-Alpine P-T estimates are shown as white ellipses and include data from the ÖC (solid ellipses), SC (dashed ellipse) and the PC (stippled ellipses).

the Variscan meta-
morphic evolution of
these rocks. In the
course of this inves-
tigation we did not
come across dis-
continuously zoned
Variscan garnets.
The only area where
discontinuous gar-
net zoning (Type 3)
occurs is a very re-
stricted area in the
ÖC only in the north-
ern vicinity of the
SC, due to the in-
creasing Eo-Alpine
metamorphic over-
print in the ÖC to-
wards the south.
This type has been
described by HOIN-
KES (1981), HOINKES
et al. (1982), HAAS
(1985), VELTMAN
(1986) and SÖLVA et
al. (2001). Discontin-
uous zoning has
also been found in
one sample of the
SC at the Schwarz-
seescharte (sample
79-3). Garnets with a
weak inverse zoning
(Type 2) were only
found in the north-
east of the ÖC, in
the base of the Per-
momesozoic Ka-
lkkögel nappe (sam-
ples 2-91, 2-16),
whereas VELTMAN
(1986) reports in-
versly zoned garnets
also in the central

Fig. 11
Compilation of the garnet zoning distribution data, based on the results of VELTMAN (1986) and RECHEIS (1998).

part of the ÖC (Fig. 6B), which is similar to TROPPER and
HOINKES (1996), who also reported inversely zoned garnets
from the southern Kaunertal area.

In contrast to this investigation, VELTMAN (1986) also re-
ports homogeneous garnets in the sillimanite zone accord-
ing to PURTSCHELLER (1969). In our study, homogeneous or
weakly zoned garnets were found mostly south of the Pas-
seier-Jaufen Line (samples 80-3, 80-15, 80-20) in the
Mauls-Meran Basement (MMB) and in the northeast of the
ÖC, underneath the Permomesozoic Kalkkögel nappe
(sample 2-76) as shown in Figure 6B. In the sillimanite
zone, we found continuously zoned garnets (samples 80-
75, 80-77, Ö-492, Ö-526). Although slight differences be-
tween the observations of VELTMAN (1986) and our investi-
gation concerning minor garnet zoning types exist, the
overall feature that most of the investigated garnets of the
ÖC show continuous growth with garnet overgrowth occur-
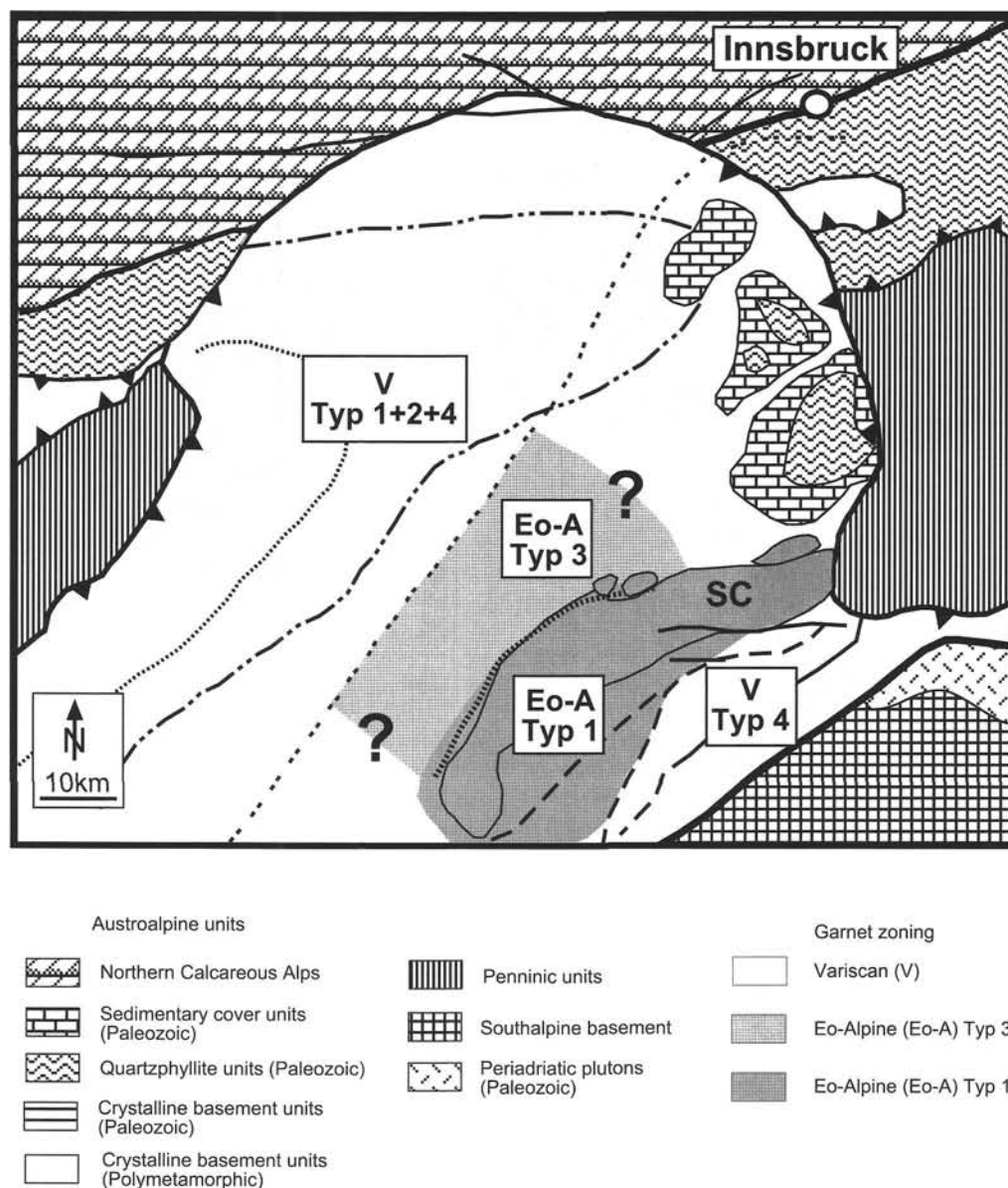ring in the ÖC north adjacent to the SC could be verified in

both studies (Fig. 11). Based on the wealth of geochrono-
logical data from this area (THÖNI, 1981, 1999), the continu-
ous garnet growth in the ÖC north of the SC can clearly be
attributed to the Variscan metamorphic cycle and the gar-
net overgrowths are Eo-Alpine in age. Continuous garnet
growth however south of the SC approaching the SAM
(southern limit of Alpine metamorphism) are of Eo-Alpine
age. Geochronological data also indicate a lack of a Permi-
an HT overprint, at least in the eastern part of the ÖC.
However, geochronological data from HAAS (1984) and re-
cent petrological investigations by SCHUSTER et al. (2001)
indicate the possibility of a Permian overprint in the Matsch
Nappe. It is also interesting to note that in the area south of
the Passeier-Jaufen Line (Meran-Mauls Basement, MMB)
only homogeneous garnets (Type 4) were found. Since this
area did not experience higher Variscan temperatures than
the western ÖC as shown in this study by petrographic
evidence (no sillimanite was found) and thermobarometric

data, these zoning patterns in the garnets cannot be due homogenization through higher temperatures, but most likely due to growth over a very small interval of the P-T path.

Previous thermobarometric investigations of the Variscan P-T conditions by VELTMAN (1986) and TROPPER and HOINKES (1996) from the different aluminiumsilicate zones within the ÖC according to PURTSCHELLER (1969) yield P-T conditions of 570-750°C and 5.8-8 kbar. At this point it must be stated that the aluminiumsilicate zones according to PURTSCHELLER (1969) cannot be interpreted as (1.) indicating the kind of aluminiumsilicate (kyanite, andalusite, sillimanite) being present at the peak of the metamorphic event and (2.) concerning the southern kyanite zone, as the result of a single metamorphic event. TROPPER and HOINKES (1996) showed for samples from the andalusite zone (southern Kaunertal) that kyanite is actually the stable aluminiumsilicate present at the peak of the Variscan metamorphic overprint. Later, during the retrograde evolution of these rocks, sillimanite (fibrolite) and andalusite grew as evident from textural relations. In this area, quartz veins containing kyanite or andalusite were also found. Thus it also seems that the proposed variscan mineral zonation seems to be a mixture of aluminiumsilicates that grew during different stages of a single metamorphic P-T path. The thermobarometric results clearly lie in the kyanite stability field. VELTMAN (1986) obtained from the northern kyanite zone 570-650°C and 4.3-7.8 kbar. For the sillimanite zone, he reported P-T conditions of 600-750°C and 4.2-6.8 kbar. TROPPER and HOINKES (1996) obtained 570-640°C and 5.8-7.5 kbar for the central andalusite zone. Our results yield P-T conditions of the northern kyanite zone of 469-630°C and 4.2-7.3 kbar and 578°C and 7.2 kbar for the southern kyanite zone. These data are well in accordance with the results from VELTMAN (1986) and TROPPER and HOINKES (1996). The data of the sillimanite zone of 621-705°C and 5.6-6 kbar also correlate well with previous estimates. One sample of the andalusite zone gave surprisingly high pressures of 8.3 kbar at 644°C (sample Ö-447). This estimate is ca. 0.8 kbar higher than the results obtained by TROPPER and HOINKES (1996). This P-T estimate was also confirmed by PERGHER (1997) by using conventional thermobarometric techniques. The other estimate of 637°C and 6.9 kbar lies well within the results of TROPPER and HOINKES (1996) and HOINKES et al. (1997).

The samples from the MMB south of the Passeier-Jaufen Line yield P-T conditions of 5.3-6.1 kbar and 540-640°C which are very similar to the Variscan P-T conditions of the ÖC. Geochronological investigations from this area by SPIESS (1995) also show that the Eo-Alpine metamorphic overprint was weak, only leading to partial rejuvenation of Variscan ages. SCHUSTER et al. (2001) argue that some of the age data from this area represent Permian cooling ages and thus these data indicate, that the obtained P-T conditions could be attributed to either the Variscan or the Permian metamorphic event. But on the other hand, petrological evidence of Permian high-temperature mineral assemblages involving sillimanite is still missing.

The Eo-Alpine P-T conditions of this investigation agree with the results of HOINKES (1981) who proposed an Eo-Alpine staurolite-in isograde in the southern ÖC with conditions of ca. 600°C and 7 kbar. These results were confirmed by our study which shows that the pressures increase in the

southern kyanite zone, east of the chloritoid-in isograde from 7.2 kbar (sample 74-1) to 8.8 kbar (sample 79-11), reaching almost 10 kbar in the SC (sample 79-3) and PC (sample 74-28). The P-T estimates from the SC by HOINKES (1986b), KONZETT and HOINKES (1991, 1996), EXNER et al. (2001), HABLER et al. (2001), KONZETT and TROPPER (2002 submitted) yield 580°C and 9-12 kbar are in very good agreement with our data from this investigation which yield 574°C and 9.8 kbar. Only one sample (75-2) shows somewhat elevated temperatures of 669°C, whereas the other samples range from 550-600°C. The lower P-T conditions of 469-485°C and 3.7-4.2 kbar were obtained from a sample (2-91) of the northeastern part of the ÖC underneath the overlying Permoscythian Kalkkögel nappe. These P-T conditions agree with the thermometric results of DIETRICH (1980, 1983), TESSADRI (1981) and PURTSCHELLER et al. (1981) as well as with the occurrence of Eo-Alpine stilpnomelane. Thermometric estimates also reveal an increase in temperature in the Permoscythian cover sequences towards the south, from 445°C in the north, reaching 530°C in the vicinity of the SC (DIETRICH, 1980, 1983; TESSADRI, 1981; PURTSCHELLER et al., 1981). This is also in good agreement with our obtained temperatures of sample 74-28 from the PC, which are 551-576°C.

Although our data do not allow any estimates of early-Variscan P-T conditions due to the lack of inclusion assemblages and the uncertainties in the Gibbs method. Petrological data from the western and central ÖC show that the first stage of the Variscan event probably was a high pressure metamorphism around 373-359 Ma, leading to the formation of eclogites in the central and western part of the ÖC (BERNHARD, 1994; MILLER and THÖNI, 1995). MOGESSIE (1984) obtained a different Variscan P-T path based on amphibole zoning patterns which reveal an early Variscan greenschist facies event. Since no geochronological evidence is reported for the early greenschist facies event, this P-T path still remains uncertain. The conditions of the eclogite facies were estimated to be 710-748°C and 26.7-27.9 kbar (MILLER and THÖNI, 1995). The dominant amphibolite facies metamorphism occurred around 330-350 Ma, as evident from Sm-Nd garnet-whole rock ages from mica schists from the western ÖC by SCHWEIGL (1993) and HOINKES et al. (1997). The garnet zoning of the samples of this investigation clearly shows that the Variscan P-T evolution was continuous, although examples for complex Variscan garnet growth were reported from the central andalusite zone by SPIESS et al. (2000).
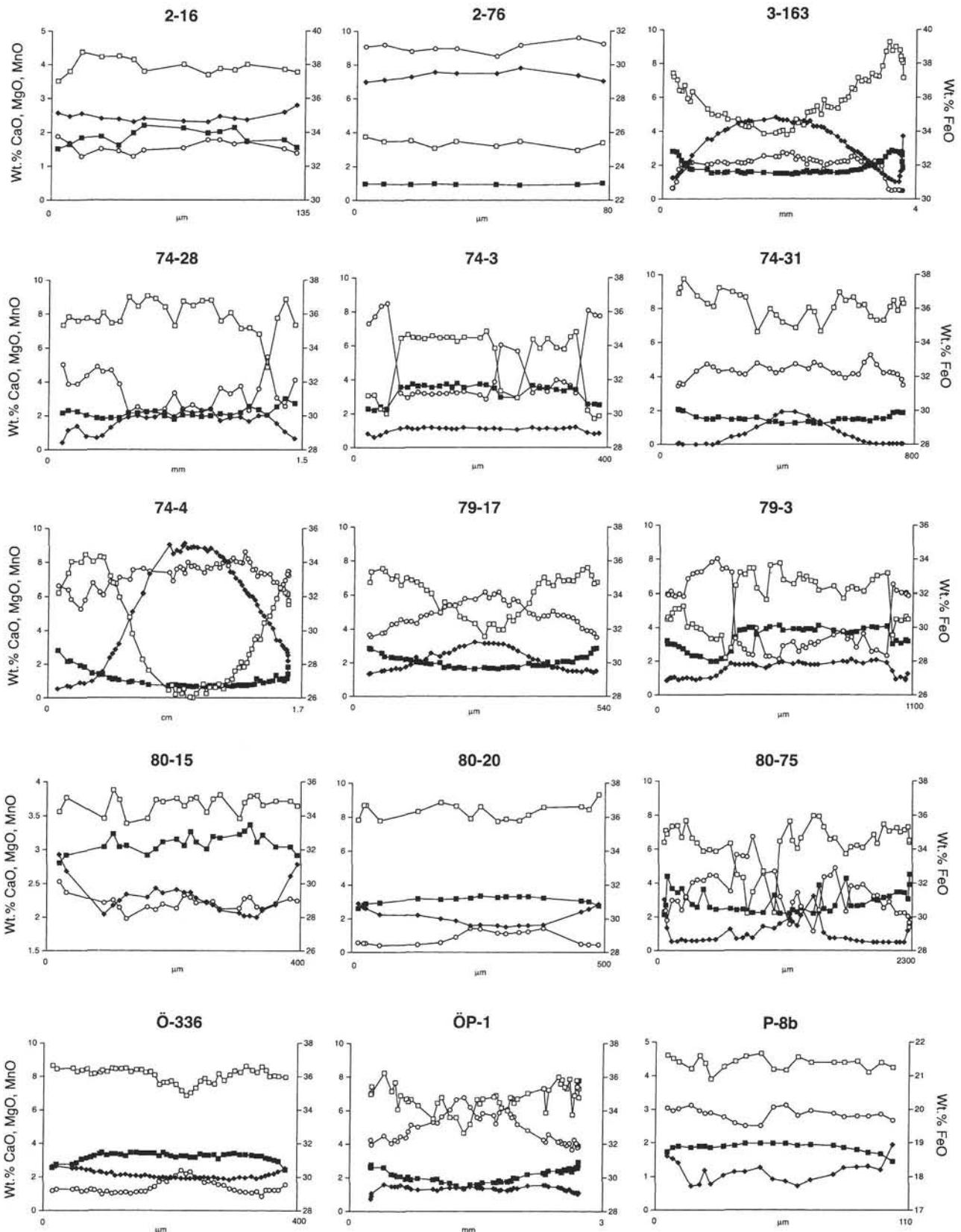
7. Acknowledgements

Appendix   →
Compilation of the garnet zoning profiles of samples, which were not displayed in Figure 4. The zoning profiles are shown not to scale for clarity.

Appendix

Legend: ○ CaO □ FeO ■ MgO ◆ MnO

Plots: 2-16, 2-76, 3-163, 74-28, 74-3, 74-31, 74-4, 79-17, 79-3, 80-15, 80-20, 80-75, Ö-336, ÖP-1, P-8b

References

BENCE, A. E. & ALBEE, A. L., 1968: Empirical correction factors of the electron microanalysis of silicates and oxides. – J. Geol., **76**, 382-403.

BERMAN, R. G., 1990: Mixing properties of Ca-Mg-Fe-Mn garnets. – Am. Mineral., **75**, 328-344.

BERNHARD, F., 1994: Zur magmatischen und metamorphen Entwicklung im westlichen Ötztal-Stubai Kristallin. – Unpubl. MSc. Thesis, Universität Graz, 315 pp.

BERNHARD, F., HOINKES, G., KAINDL, R., LICHEM, C., SCHWEIGL, J., THÖNI, M. & TROPPER, P., 1993: Petrologische und geochemische Untersuchungen im westlichen Ötztal-Stubai-Kristallin (Kaunertal-Langtaufers). – Mitt. Öster. Mineral. Ges., **138**, 143-151.

BJERG, S. C., MOGESSIE, A. & BJERG, E., 1992: HYPER FORM – a hypercard program for the MacIntosh microcomputers to calculate mineral formulae from electron microprobe and wet chemical analyses. – Comp. Geosci., **18**, 717-745.

CHOWANETZ, E., 1990: Der Winnebachmigmatit (Ötztal/Tirol): Argumente fur eine altpaläozoische Anatexis. – Unpubl. Masters Thesis, Universität Wien, 78 pp.

CHOWANETZ, E., 1991: Strukturelle und geochronologische Argumente für eine altpaläozoische Anatexis im Winnebachmigmatit (Ötztal/Tirol, Österreich). – Mitt. Ges. Geol. Bergbaustud. Öster., **37**, 15-36.

CHOWANETZ, E., 1994: The age of the Ötztal migmatites – still a matter of debate. – Mitt. Öster. Mineral. Ges., **139**, 284-286.

DIETRICH, H., 1980: Mineralogisch-petrographische Untersuchungen zur Metamorphose des Brennermesozoikums. – Unpubl. Ph.D. Thesis, University of Innsbruck, 173 pp.

DIETRICH, H., 1983: Zur Petrologie und Metamorphose des Brennermesozoikums (Stubaier Alpen, Tirol). – TMPM, **31**, 237-257.

ESSENE, E. J., 1982: Geologic thermometry and barometry. In Ferry JM (ed.) Characterization of metamorphism through mineral equilibria. – Rev. Mineral., **10**, 152-206.

ESSENE, E. J., 1989: The current status of thermobarometry in metamorphic rocks. – In: J. S. DALY, R. A. CLIFF, B. W. D. YARDLEY (eds.): Evolution of metamorphic belts. Geol. Soc. Lon. Spec. Publ., **43**, 1-44.

EXNER, U., FUSSEIS, F., GRASEMANN, B., HABLER, G., LINNER, M., SÖLVA, H., THIEDE, R. & THÖNI, M., 2001: Cretaceous eclogite-facies metamorphism in the Eastern Alps: New Insights, data and correlations from an interdisciplinary study. – J. Conf. Abstr., 6/1, 387.

FERRY, J. M. & SPEAR, F. S., 1978: Experimental calibration of the partitioning of Fe and Mg between garnet and biotite. – Contrib. Mineral. Petrol., **66**, 113-117.

FRANK, W., HOINKES, G., PURTSCHELLER, F. & THÖNI, M., 1987: The Austroalpine unit west of the Hohe Tauern: the Ötztal-Stubai complex as an example for the Eo-Alpine metamorphic evolution. – In: H. W. FLÜGEL & P. FAUPL (eds.) Geodynamics of the Eastern Alps, Franz Deuticke Verlag Wien: 280-320.

FREY, M., DESMONS, J. & NEUBAUER, F., 1999: The new metamorphic map of the Alps; 1:50000; 1:100000. – SMPM, **79**, 230 pp.

GORDON, T. M., 1992: Generalized thermobarometry: solution of the inverse chemical equilibrium problem using data for individual species. – Geochim. Cosmochim. Acta, **56**, 1793-1800.

GORDON, T. M., 1998: WEBINVEQ thermobarometry; an experiment in providing interactive scientific software on the World Wide Web. – Comp. Geosci., **24**, 43-49.

HAAS, R., 1985: Zur Metamorphose des südlichen Ötztalkristallins unter besonderer Berücksichtigung der Matsche Einheit (Vintschgau/Südtirol). – Unpubl. Ph.D. Thesis, University of Innsbruck, 118 pp.

HABLER, G., LINNER, M., THIEDE, R. & THÖNI, M., 2001: Eo-Alpine Andalusite in the Schneeberg Complex (Eastern Alps, Italy/Austria): Constraining the P-T-t-D Path during Cretaceous Metamorphism. – J. Conf. Abstr., **6**, 340.

HOINKES, G., 1981: Mineralreaktionen und Metamorphosebedingungen in Metapeliten des westlichen Schneebergerzuges und des angrenzenden Altkristallins (Ötztaler Alpen). – TMPM, **28**, 31-54.

HOINKES, G., 1986a: Eoalpine metamorphism of the Austroalpine Schneeberg-Complex and the adjacent Ötztal crystalline basement (summary). – SMPM, **66**, 135-138.

HOINKES, G., 1986b: Effect of grossular-content in garnet on the partitioning of Fe and Mg between garnet and biotite. – Contrib. Mineral. Petrol., **92**, 393-399.

HOINKES, G., PURTSCHELLER, F. & TESSADRI, R., 1982: Polymetamorphose im Ostalpin westlich der Tauern (Ötztaler Masse, Schneebergerzug, Brennermesozoikum). – Geol. Paläont. Mitt. Univ. Innsbruck, **12**, 95-113.

HOINKES, G., KOSTNER, A. & THÖNI, M., 1991: Petrologic constraints for Eo-Alpine eclogite facies metamorphism in the Austroalpine Ötztal Basement. – Mineral. Petrol., **43**, 237-254.

HOINKES, G. & THÖNI, M., 1993: Evolution of the Ötztal-Stubai, Scarl-Campo and Ulten basement units. – In: J. F. VON RAUMER & F. NEUBAUER (eds.) Premesozoic Geology in the Alps, Springer Verlag, Heidelberg, 485-494.

HOINKES, G., THÖNI, M., BERNHARD, F., KAINDL, R., LICHEM, C., SCHWEIGL, J., TROPPER, P. & COSCA, M., 1997: Metagranitoids and associated metasediments as indicators for the pre-Alpine magmatic and metamorphic evolution of the Western Austroalpine Ötztal Basement (Kaunertal, Tirol). – SMPM, **77**, 299-314.

HOINKES, G., KOLLER, F., RANTITSCH, G., DACHS, E., HÖCK, V., NEUBAUER, F. & SCHUSTER, R., 1999: Alpine metamorphism of the Eastern Alps. – SMPM, **79**, 155-181.

HOLLAND, T. J. B. & POWELL, R., 1998: An internally-consistent thermodynamic data set for phases of petrological interest. – J. Metam. Geol., **8**, 89-124.

KAINDL, R., 1995: Präalpidische magmatische und metamorphe Entwicklung im westlichen Ötztal-Stubai-Kristallin (Kaunertal-Tirol). Unpubl. Masters Thesis, University of Graz, 170 pp.

KAINDL, R., HOINKES, G., KNOLL, P. & ABART, R. 1999: Fluid inclusions related to Variscan and Alpine metamorphism in the Austroalpine Ötztal Basement, Eastern Alps. – Mineral. Petrol, **65**, 29-49.

KLÖTZLI-CHOWANETZ, E., 2001: Migmatite des Ötztalkristallins – Petrologie und Geochronologie. Unpubl. Ph.D. Thesis, University of Vienna, 155 pp.

KLÖTZLI-CHOWANETZ, E., KLÖTZLI, U. & KOLLER, F., 1997: Lower Ordovician migmatisation in the Ötztal crystalline basement (Eastern Alps, Austria): linking U-Pb and Pb-Pb dating with zircon morphology. SMPM, **77**, 315-324.

KÖHLER, M., 1978: Brennerflachbahn Projekt 1978: Ergebnisse der geologischen Untersuchungen. – Geol. Paläont. Mitt. Univ. Innsbruck, **8**, 1-99.

KONZETT, J. & HOINKES, G., 1991: High pressure metamorphism in the Austroalpine Schneeberg Complex and adjacent Ötztal basement rocks. – Terra Abstracts, **3**, 88.

KONZETT, J. & HOINKES, G., 1996: Paragonite-hornblende assemblages and petrological significance: an example from the Austroalpine Schneeberg Complex, Southern Tyrol, Italy. – J. Metam. Geol., **14**, 85-101.

KRETZ, R., 1983: Symbols for rock-forming minerals. – Am. Mineral., **68**, 277-279.

LICHEM, C., 1993: Petrologische und geochemische Untersuchungen an Orthogneisen des westlichen Ötztal-Stubai Kristallins (Kaunertal). Unpubl. Masters Thesis, University of Graz, 139 pp.

MILLER, C. & THÖNI, M., 1995: Origin of eclogites from the Austroalpine Ötztal basement (Tirol, Austria): geochemistry and Sm-Nd vs. Rb-Sr isotope systematics. – Chem. Geol., **122**, 199-225.

MOGESSIE, A., 1984: Petrology and geochemistry of the Ötztal-Stubai amphibolites. – Unpubl. Ph.D. Thesis, University Innsbruck, 147 pp.

NEUBAUER, F., HOINKES, G., SASSI, F. P., HANDLER, R., HÖCK, V., KOLLER, F. & FRANK, W., 1999: Pre-Alpine metamorphism in the Eastern Alps. – SMPM, **79**, 41-62.

PERGHER, L., 1997: Kristallingeologische und petrologische Untersuchungen im vorderen Pitztal (Wildgrat, Zaunhof, Aifenspitze). – Unpubl. Masters Thesis, University of Innsbruck, 87 pp.

PURTSCHELLER, F., 1969: Petrographische Untersuchungen an Alumosilikatgneisen des Ötztales-Stubaier Altkristallins. – TMPM, **13**, 35-54.

PURTSCHELLER, F., HOINKES, G., DIETRICH, H., RAMMELMAIER, D. & TESSADRI, R., 1981: T-Bedingungen der alpidischen Metamorphose im Ostalpin westlich der Tauern. – Fortschr. Mineral., **59**, Beiheft 1, 161-162.

RECHEIS, A., 1998: Chemische Granatzonierungen und PT Bestimmungen an metapelitischen Gesteinen des Ötztal-Stubai-Altkristallins. – Unpubl. Masters Thesis, University of Innsbruck, 97 pp.

SCHUSTER, R., SCHARBERT, S., ABART, R. & FRANK, W., 2001: Permo-Triassic extension and related HAT/LP metamorphism in the Austroalpine – Southalpine realm. – Mitt. Ges. Geol. Bergbaustud. Öster., **45**, 112-141.

SCHWEIGL, J., 1993: Kristallingeologische Untersuchungen in den Nauderer Bergen (Westliche Ötztaler Alpen, Tirol). – Unpubl. Masters Thesis, University of Vienna, 87 pp.

SCHWEIGL, J., 1995: Neue geochronologische und isotopengeologische Daten zur voralpidischen Entwicklungsgeschichte im Ötztalkristallin (Ostalpen). – Jb. Geol. BA., **138/1**, 131-149.

SÖLLNER, F., 1982: Zur Altersstellung des Winnebach-Migmatits im Ötztal (Ostalpen). – Verh. Geol. BA., **2**, 95-106.

SÖLLNER, F. & HANSEN, B. T., 1987: „Pan-afrikanisches" und „kaledonisches" Ereignis im Ötztal-Kristallin der Ostalpen: Rb-Sr- und U-Pb-Altersbestimmungen an Migmatiten und Metamorphiten. – Jb. Geol. BA., **130/4**, 529-569.

SÖLLNER, F. & SCHMIDT, K., 1981: Rb/Sr- und U/Pb-Datierungen am Winnebach-Migmatit (Ötztaler Alpen, Österreich). – Fortschr. Mineral., **59**, Beiheft 1, 188.

SÖLVA, H., THÖNI, M., GRASEMAN, B. & LINNER, M., 2001: Emplacement of eo-Alpine high-pressure rocks in the Austroalpine Ötztal complex (Texel group, Italy/Austria). – Geodinamica Acta, **14**, 345-360.

SPEAR, F. S., 1993: Metamorphic phase equilibria and pressure-temperature-time paths. – Mineral. Soc. Amer. Monograph, 799 pp.

SPEAR, F. S., KOHN, M. J., FLORENCE, F. P. & MENARD, T., 1991a: A model for garnet and plagioclase growth in pelitic schists: implications for the thermobarometry and P-T path determinations. – J. Metam. Geol., **8**, 683-696.

SPEAR, F. S., PEACOCK, S. M., KOHN, M. J., FLORENCE, F. P. & MENARD, T., 1991b: Computer programs for petrologic P-T-t path calculations. – Am. Mineral., **76**: 2009-2013.

SPIESS, R., 1995: The Passeier-Jaufen Line: a tectonic boundary between Variscan and eo-Alpine Meran-Mauls basement. – SMPM, **75**, 413-425.

SPIESS, R., BERTOLO, B., BORGHI, A., CHINELLATO, M. & TINOR CENTI, M., 2000: Microtextures of opaque inclusions: their use as indicators for hiatuses during garnet porphyroblast growth. – J. Metam. Geol., **18**, 591-603.

TESSADRI, R., 1981: Metamorphose am Ostende des Schneeberger Zuges (Sterzing, Südtirol). – Unpubl. Ph.D. Thesis, University of Innsbruck, 95 pp.

THÖNI, M., 1981: Degree and evolution of the Alpine metamorphism in the Austroalpine unit west of the Hohe Tauern in the light of K/Ar and Rb/Sr age determinations on micas. – Jb. Geol. BA., **124**, 111-174.

THÖNI, M., 1986: The Rb-Sr thin slab isochron method – an unreliable geochronologic method for dating geologic events in polymetamorphic terrains? – Mem. Sci. Geol., **38**, 283-352.

THÖNI, M., 1999: A review of geochronological data from the Eastern Alps. – SMPM, **79**, 209-230.

TRACY, R. J., 1982: Compositional zoning and inclusions in metamorphic minerals. – In: J. M. FERRY (ed.) Characterization of metamorphism through mineral equilibria, Rev. Mineral., **10**, 355-394.

TROPPER, P., 1993: Petrologische Untersuchungen an Metapeliten und Amphiboliten des westlichen Ötztal-Stubai Kristallins (Kaunertal). – Unpubl. Masters Thesis, University of Graz, 152 pp.

TROPPER, P. & HOINKES, G., 1996: Thermobarometry in Al_2SiO_5-bearing metapelites in the western Austroalpine Ötztal-basement. – Mineral. Petrol, **58**, 145-170.

VELTMAN, C. B., 1986: Zur Polymetamorphose metapelitischer Gesteine des Ötztal Stubaier Altkristallins. – Unpubl. Ph.D. Thesis, University of Innsbruck, 164 pp.